Putting the Par back into ParABS: Plasmid Partitioning Driven by ParA Oscillations

Robin Köhler, Seán M. Murray*

Max Planck Institute for Terrestrial Microbiology and LOEWE Centre for Synthetic Microbiology (SYNMIKRO), Karl-von-Frisch Straße 14, 35043 Marburg, Germany

*Email: sean.murray@synmikro.mpi-marburg.mpg.de

Abstract

The ParABS system is crucial for the faithful segregation and inheritance of many bacterial chromosomes and low-copy number plasmids. However, despite extensive research, the spatio-temporal dynamics of the ATPase ParA and its connection to the dynamics and positioning of the ParB-coated cargo has remained unclear. In this study, we utilise high-throughput imaging, quantitative data analysis, and computational modelling to explore the *in vivo* dynamics of F-plasmid ParA and its interaction with ParB-coated plasmids and the nucleoid. As previously observed, we find that ParA undergoes collective migrations ('flips') between cell halves multiple times per cell cycle, resulting in oscillations over time. We reveal that a constricted nucleoid is required for these migrations and that they are triggered by a plasmid crossing into the cell half with greater ParA. Using simulations, we show that these dynamics can be explained by the combination of nucleoid constriction and cooperative ParA binding to the DNA, in line with the behaviour of other ParA proteins. We further show that these ParA flips act to equally partition plasmids between the two lobes of the constricted nucleoid and are therefore important for plasmid stability, especially in fast growth conditions for which the nucleoid constricts early in the cell cycle. Overall our work sheds light on a second mode of action of the ParABS system and deepens our understanding of this important system.

Introduction

In bacterial cell division, the precise segregation and positioning of genetic material is essential for its faithful inheritance. However, with only a few plasmids per cell, random positioning cannot ensure the stability of low copy-number plasmids and an active partitioning system is required. For this, many plasmids use the widespread ParABS partitioning system (Gerdes et al., 2000; Mishra and Srinivasan, 2022), composed of three components: (i) *parS*, a centromere-like binding site, (ii) ParA, a deviant Walker-type ATPase, and (iii) ParB, a protein that binds to the *parS* site. ParA, in its dimeric ATP-bound state, binds DNA non-specifically, coating the nucleoid of the cell (Ebersbach and Gerdes, 2001; Lim et al., 2005). It detaches from the DNA upon hydrolysis and requires a prolonged cytosolic conformational transition before again becoming competent for binding (Chodha et al., 2023; Vecchiarelli et al., 2010). ParB, which also dimerizes, binds to *parS* and spreads out along the DNA for several kilobases to form the nucleoprotein 'partition complex', visible using fluorescent microscopy (Hirano et al., 1998; Rodionov et al., 1999). Very recently, it was found that the ParB of several species/plasmids is a CTPase that can entrap and slide along the DNA, potentially explaining

the observed spreading (Antar et al., 2021; De Asis Balaguer et al., 2021; Jalal et al., 2021, 2020; Osorio-Valeriano et al., 2021, 2019; Soh et al., 2019; Taylor et al., 2021). ParB also stimulates the ATPase activity of ParA, generating a local depletion of ParA-ATP around the plasmid (Hatano et al., 2007; Ringgaard et al., 2009; Vecchiarelli et al., 2014a). The resulting ParA-ATP gradient, shaped by both the nucleoid and the plasmids is then believed to direct plasmid movement and result in the regular (equi-distant) positioning of plasmids across the length of the cell (Hatano et al., 2007; Hatano and Niki, 2010; Ringgaard et al., 2009; Vecchiarelli et al., 2010).

At the molecular level, the central hypothesis for how directed movement occurs is the existence of protein tethers between ParB bound to the cargo (the *parS*-proximal DNA of the plasmid or chromosome) and non-specifically bound ParA-ATP on the underlying nucleoid. The creation of these tethers, which are transient due to ParB stimulated hydrolysis, depends on the local concentration of nucleoid-bound ParA such that more tethers are created in the direction of increasing ParA concentration, thereby providing a means for the cargo to sense the gradient (Ietswaart et al., 2014; Sugawara and Kaneko, 2011). The pulling force itself is believed to be generated by the elastic fluctuations of the DNA and/or the protein tethers as suggested by computational modelling (Hu et al., 2017, 2015; Lim et al., 2014; Surovtsev et al., 2016a).

However, while *in vitro* reconstitutions support this view (Hwang et al., 2013; Vecchiarelli et al., 2014a, 2013), the nature of the plasmid movement *in vivo* and its connection to ParA are much less understood. First, regarding the plasmid, while both oscillatory and defined positioning have been described, the prevalence of either mode within and across species was unclear (Ebersbach et al., 2006; Hatano et al., 2007; Ringgaard et al., 2009; Sengupta et al., 2010). In this direction, we recently used high-throughput imaging and analysis to quantify the dynamics of F-plasmid and found that it is elastically 'pulled' to defined locations within the cell (mid-cell for a single plasmid, the quarter positions for two plasmid) (Köhler et al., 2022). However, at the lowest plasmid concentrations (typically a single plasmid in a long cell) the dynamics become oscillatory in nature. This was even more pronounced for the unrelated plasmid pB171 harbouring a distantly related ParABS system, which exhibits clear oscillatory dynamics across the length of the cell in almost all cells containing a single plasmid (Köhler et al., 2022).

Several models that can explain (typically a subset of) the observed plasmid dynamics have been proposed, both separately from (Ietswaart et al., 2014; Jindal and Emberly, 2019; Sugawara and Kaneko, 2011; Walter et al., 2017) and including (Hu et al., 2017; Surovtsev et al., 2016a), the molecular mechanism of force generation. We combined aspects of these models into a new stochastic model that could produce all the dynamical regimes within a single unifying model (Köhler et al., 2022). Critical for this was the understanding of the importance of the length-scale of ParA diffusion on the nucleoid as the primary parameter controlling the transition between oscillatory dynamics and targeted positioning. However, while a quantitative comparison of this model with measurements of F plasmid gave remarkable agreement, a similar comparison to the ParA distribution was not performed.

Indeed, the dynamics of ParA and its correlation to plasmid movement has remained one of the least understood aspects of this system. While plasmids have been observed to follow a retracting gradient of ParA across the cell (Hatano et al., 2007; Hatano and Niki, 2010; Ringgaard et al., 2009) similar to an *in vitro* reconstitution (Vecchiarelli et al., 2014a), the connection between the two components in individual cells is often unclear. In particular, the ParA of F plasmid, TP228 and most recently ParA2 of *Vibrio cholerae* have been observed to oscillate, or flip, between the two halves of the cell (Ah-Seng et al., 2013; Chodha et al., 2023; McLeod et al., 2017). However, none of the current

models, including our own, can reproduce this behaviour, indicating a fundamental gap in our understanding of how this system functions.

Here, we investigate ParA dynamics and its connection to F plasmid movement using a combination of high-throughput imaging and quantitative data analysis. We find that ParA flips between the two cell halves appear to be triggered by the movement of a plasmid from the cell half with the least ParA to the cell half with the most. This is most likely to occur when there is an asymmetry in the amount of plasmids/ParB in each cell half and the effect of the flips is to encourage equi-partitioning between the cell halves. Importantly, asymmetry in ParA, and hence flips, only occurs after the nucleoid has begun to constrict. Building on our previous stochastic model of plasmid positioning, we show that this behaviour can be explained by cooperative ParA binding to the nucleoid as has already been suggested for other ParA proteins (Baxter et al., 2020; Chodha et al., 2023; Hester and Lutkenhaus, 2007; McLeod et al., 2017), and for membrane recruitment of the ParA-like protein MinD (Hu et al., 2002; Lackner et al., 2003), which also exhibits oscillatory dynamics. Using our model, we demonstrate that ParA flipping reduces plasmid loss in conditions with early nucleoid constriction by ensuring partitioning of plasmids between the two lobes of the nucleoid. This is important as plasmid replication is most likely to occur on the nucleoid lobe with the most plasmids, thereby reinforcing any asymmetry. Thus the ParABS system has two modes of action to effect plasmid stability: 1) regular positioning of plasmids on (each) nucleoid mass and 2) equi-partitioning of plasmids between the two lobes of the constricted nucleoid. Ultimately, our findings provide a comprehensive understanding of ParA oscillations and their functional significance within the ParABS system.

Results

ParA flips abruptly between cell halves

To study the dynamics of F plasmid ParA and its relationship to plasmid positioning and the cell cycle, we used our previously developed high-throughput microfluidic and image analysis pipeline (Köhler et al., 2022) (Figure S1). We visualised the two protein components using an F plasmid derivative carrying endogenous fluorescent fusions of ParA and ParB (ParA-mVenus, ParB-mTurquoise2) (Guilhas et al., 2020). The nucleoid of the host *E. coli* cell was also imaged using chromosomally expressed HU-mCherry (Guilhas et al., 2020). A representative cell cycle is shown in Figure 1A. We found that while ParA is distributed relatively uniformly at birth, later (at ~30 min in the example shown) it often undergoes collective migrations between the two halves of the cell, consistent with previous reports (Ah-Seng et al., 2013; Hatano et al., 2007).

To quantify ParA asymmetry, we first measured the fractional difference A_A in the ParA-mVenus signal between each half of the cell (Figure 1B). Interestingly, we found this to increase significantly with cell length, particularly between the average birth and division lengths of 3 µm and 6 µm respectively (Figure 1C, S1D). By defining ParA to be in an asymmetric state when at least ⅔ of the signal originates from one cell half (an absolute asymmetry $|A_A| > 0.33$), we could also identify the collective migration events (which we call 'flips') by the switching of ParA between asymmetric states (Figure S2A). According to this definition, cells typically display two flips during their cell cycle (Figure S2B), occurring, on average, 20 minutes apart but with substantial variation (Figures S2C). The time between these flips lengthens as the cell grows (Figure 2SD), suggesting that the asymmetric state becomes increasingly stable (less likely to flip) as the cell grows. ParA asymmetry at division often results in one daughter cell inheriting the majority of ParA, producing a very heterogeneous

distribution of in newborn cells: on average one daughter cell inherits 73% of the ParA signal (Figure S2E). However, the presence of flips appeared to be independent of ParA levels (Figure S3).

The example cell cycle shown in Figure 1A also highlights another feature of ParA dynamics. During a flipping event, the ParA signal decreases uniformly in one half, while simultaneously increasing uniformly in the other. Although in some cells, the gradient did appear to retract at times, this was not consistent and when we averaged over many flipping events, we found that the migration between the two cell halves to be uniform (Figure 1D) and we confirmed this by imaging cells on an agarose pad at higher time resolutions (Figure S4). The migration occurs rapidly, taking only a few minutes for the majority of ParA to migrate from one cell half to the other.

In essence, F plasmid ParA exhibits an asymmetrical distribution and rapid, uniform transitions between cell halves during the later stages of the cell cycle. This asymmetry often results in one daughter cell inheriting a significant majority of ParA, explaining the heterogeneous distribution of ParA in newborn cells.

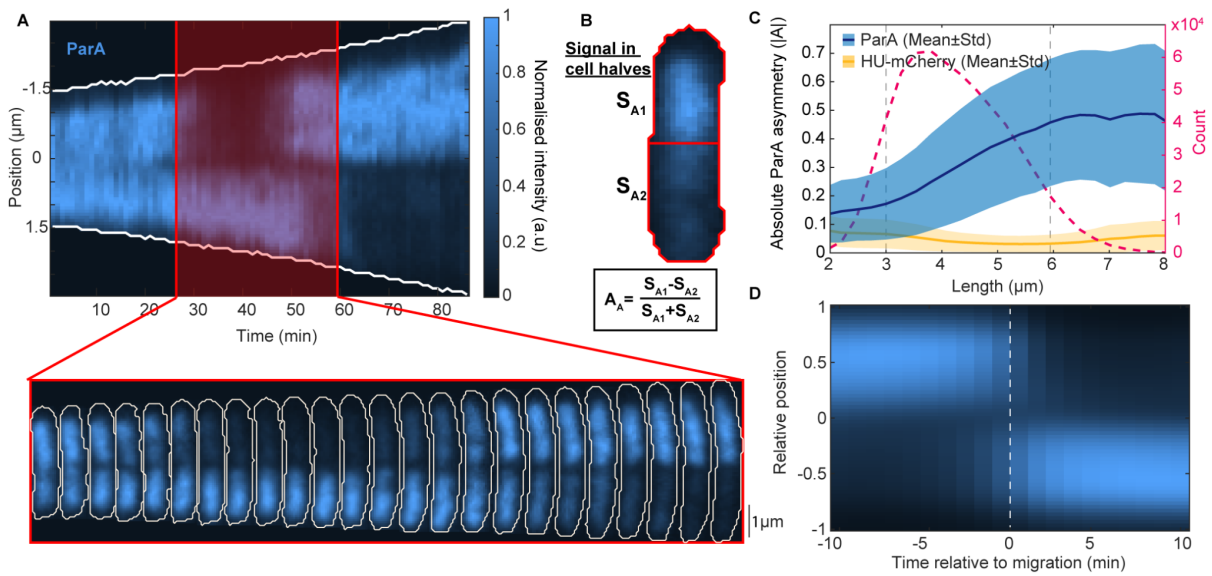

Figure 1. Characterising ParA migration events and their dependence on plasmid movements. **(A)** Top: Intensity profile of ParA-mVenus along the long axis of one cell (1 minute time intervals). Bottom: Single cell overview of the red highlighted region. **(B)** The ParA-mVenus signal in each half (S_{A1}, S_{A2}) is used to calculate the ParA asymmetry: $A_A = \frac{S_{A1}-S_{A2}}{S_{A1}+S_{A2}}$. A value of 0 corresponds to an even distribution, +1/-1 correspond to all of the signal coming from one or the other cell half. **(C)** Blue: Absolute ParA asymmetry of cells plotted against length (mean ± SD). Orange: Absolute asymmetry of the nucleoid (HU-mCherry). Red: Number of data points at each length. **(D)** Average kymograph of all ParA flips aligned by the moment the flip occurred. Length was normalised such that +1/-1 correspond to the poles of the cell. Furthermore, the cells were orientated such that the majority of ParA is in the same cell half before the flip. Panel **(C)** was generated from 5219 cell cycles and panel **(D)** was generated from 2537 flipping events.

ParA asymmetry increases upon nucleoid constriction

We next investigated what underlies the increase of ParA asymmetry with cell length (Figure 1C). Since ParA flips from one cell half to the other, it suggested that the mid-cell constriction of the nucleoid may play a role. Indeed, we found ParA asymmetry to be stronger and more frequent after the nucleoid constricts (Figure 2A, S3). To quantify this, we first set a threshold depth to characterise

dips in the HU-mCherry signal as being constrictions (Figure S5). Since the nucleoid is dynamic and shallow constrictions can be transient, we then determined, for each cell cycle, the onset of nucleoid constriction i.e. the time point from which a constriction deeper than the threshold is continuously present for the remainder of the cell cycle. We found while ParA asymmetry remains constant before nucleoid constriction begins, it increases abruptly afterwards (Figure 2B). Furthermore, the dependence on cell length was much weaker before the onset of constriction than afterwards (Figure 2C), indicating that nucleoid constriction rather than cell length directly is the more important factor for ParA asymmetry. Note that ParA could still exhibit significant asymmetry before constriction, as quantified by a comparison to the asymmetry value of the HU-mCherry nucleoid signal which is largely symmetrical (Figure 2B). This pre-constriction asymmetry was often apparent visually (Figure 2A, S3) consistent with previous studies (Hatano et al., 2007). Thus the asymmetry caused by ParA flips between nucleoid lobes is in addition to its asymmetry within each lobe.

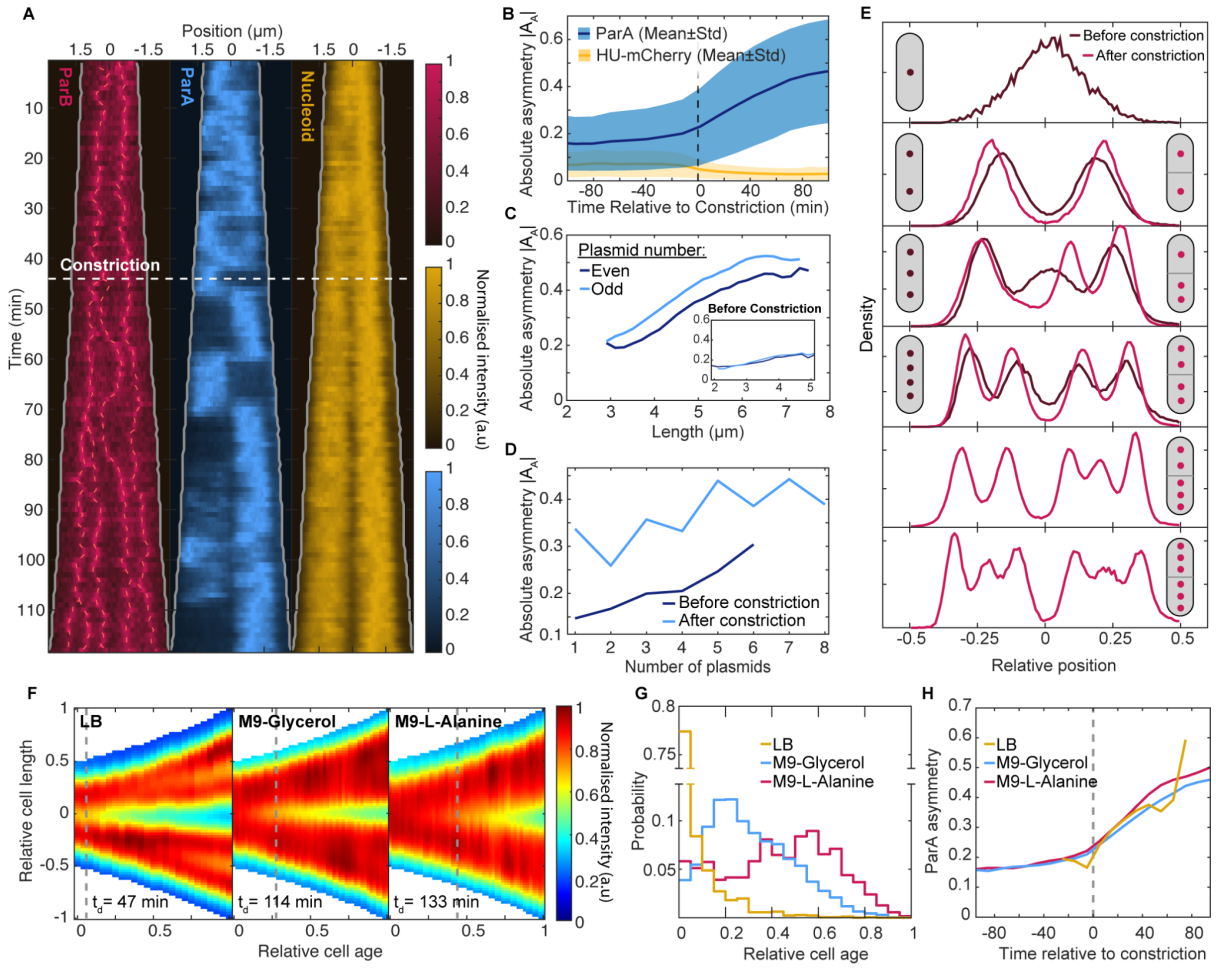

Figure 2. Nucleoid constriction is necessary for stable ParA oscillations. **(A)** Kymograph of Nucleoid (HU-mCherry), ParA-mVenus, ParB-mTurquoise2 of a cell. Red dashed lines indicate tracked foci. The white dashed line denotes the first frame in which the nucleoid constriction was detected. **(B)** Average ParA (blue) and nucleoid (orange) asymmetry relative to nucleoid constriction (mean ± std). **(C)** The absolute asymmetry of ParA in cells containing varying numbers of plasmids after and before (inset) the formation of nucleoid constriction. **(D)** The absolute asymmetry of ParA in cells with different numbers of plasmids after the formation of the nucleoid constriction. **(E)** Histograms of the distribution of plasmids before (dark red) and after (red) constriction formation. Cells after the formation of the nucleoid constriction are aligned such that the side with the most plasmids is consistent across each cell, as depicted in the cartoon on the right side. **(F)** Kymographs of the nucleoid in three different growth conditions. The different colour scale used here was chosen for visual clarity. **(G)** Distribution of the timing of nucleoid constriction formation. **(H)** Mean ParA asymmetry as in panel **(B)** for all three growth

conditions studied. The data in panels **(A)-(E)** is from the M9-Glycerol condition as in Figure 1. Number of cell cycles used: 5219 (M9-Glycerol), 606 (LB) and 569 (M9-L-Alanine).

Interestingly, we found that ParA asymmetry is slightly but consistently higher after constriction in cells with an odd number of plasmids (Figure 2C). We examined this in more detail by organising cells according to the number of plasmids they contain and their distribution within the cell (Figure 2D,E). Due to the ParABS system, plasmids tended to be as evenly distributed as possible between the two cell halves. However, since plasmids are associated to nucleoid regions of higher DNA density due to their tethering by non-specifically bound ParA (Le Gall et al., 2016), there is a natural bias for them to move away from the nucleoid constriction site. Therefore in cells with an odd number of plasmids, the central plasmid is not positioned at mid-cell after constriction but within one or the other nucleoid lobe, leading to an unequal number of plasmids in each lobe. This could be clearly seen in cells with three plasmids, for which there is sufficient data before and after nucleoid constriction (Figure 2E). Since plasmid-associated ParB stimulates hydrolysis and DNA unbinding of ParA, we speculated that this unequal plasmid partitioning would result in increased ParA asymmetry and our measurements were consistent with this (Figure 2C,D). Indeed, we found that the average ParA asymmetry showed a zig-zag dependence on plasmid number with higher values for odd numbers (Figure 2D).

If the onset of nucleoid constriction is indeed a requirement for ParA flipping, then the relationship to ParA asymmetry should be maintained even when the nucleoid constricts earlier or later in the cell cycle. We therefore repeated our measurements with cells grown on a poorer carbon source (M9-L-alanine) and in richer media (LB). In the latter case, nucleoid constriction begins shortly after birth or already in the previous cell cycle, whereas using L-alanine constriction occurs about halfway through the cell cycle. Our default M9-Glycerol condition lies somewhere in between (Figure 2F,G). We found in both cases ParA asymmetry begins to increase noticeably upon the onset of nucleoid constriction (Figure 2H). Interestingly, the curves of all three conditions collapsed onto each other when arranged according to the time of constriction onset. We speculate this is due to similar progression of the replication forks and, correspondingly, the progression of nucleoid constriction and hence ParA asymmetry increases similarly across the three conditions. Overall, these results identify nucleoid constriction as an important factor for ParA dynamics. We will investigate the connection to plasmid maintenance in the next sections.

Plasmid-bound ParB triggers ParA migration

Consistent with the observed higher ParA asymmetry in cells with unequal plasmid partitioning, we noticed that in many cell cycles ParA flipping was coincident with a plasmid moving from one half of the cell to the other (Figure 3A, also Figures 2A, S2A, S3). To quantify this, we next analysed plasmid movement and replication in the ten minutes preceding each flip (Figure 3B-F). We found that in 53% of cases, a plasmid could be observed to cross the mid-cell before ParA flipped, while in 18% there was a plasmid replication event, which also changes the difference in plasmid number between the two cell halves (there was 8% overlap of these populations). For the remaining 37%, no change in the plasmid distribution was detected. Indeed ParA could be asymmetric and flip even when plasmids were equally partitioned (Figure 3E).

Focusing on plasmid midcell-crossing events, in 91% of cases, the plasmid moves from the cell half with the least ParA to the cell half with the most (Figure 3G) and the crossing coincides with the time of maximum ParA asymmetry. On average, the asymmetry then decreases, reaching parity 5 minutes after the crossing event (Figure 3H). This was predominantly due to crossings that reversed the

asymmetry in the number of plasmids, which occurs when there is an odd total number of plasmids (Figure 3I). The average ParA asymmetry decreased more slowly when the number of plasmids in the two cell halves was equalised by the crossing event indicating flips were less likely to occur. Given that the predominant configuration in cells with unequal plasmid partitioning has ParA distributed more to the cell half with fewer plasmids (Figure 3J), the data indicates an ordering for the plasmid-crossing-induced flipping of ParA (Figure 3K). Specifically, a plasmid from the cell half with the majority of plasmids moves to the other half of the cell where the ParA concentration is greatest. The resulting relocation of plasmid-bound ParB induces ParA to rapidly flip to the other cell-half reestablishing the initial configuration, presumably through its stimulation of ParA hydrolysis and facilitated by the constriction of the nucleoid.

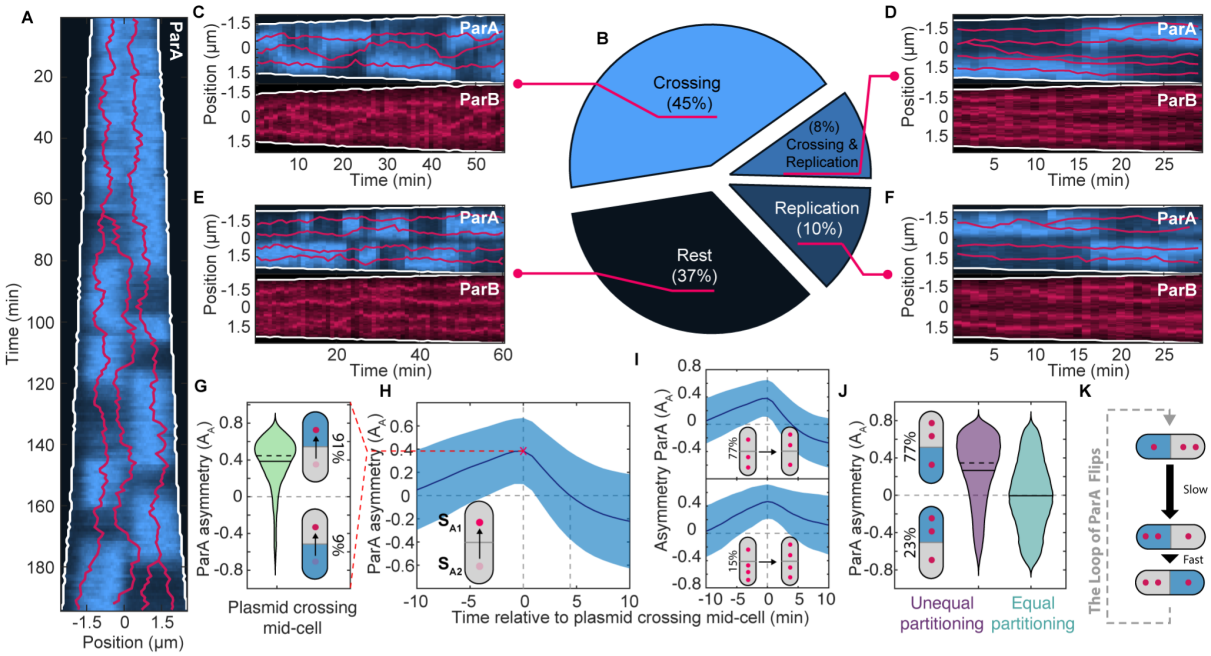

Figure 3. What precedes a migration event. **(B)** Pie chart of what cellular event precedes (within 10 min) a ParA migration event. Crossing: A plasmid crossing mid cell. Replication: A plasmid is replicated. Rest: Neither crossing nor replication. **(C)-(F)** An example portion of a cell cycle in which the indicated event preceded ParA migration. **(G)** Distribution of ParA at the time of a plasmid crossing event. **(H)** Averaged ParA asymmetry over all plasmid crossing events from -10 to 10 minutes, with 0 marking the moment a plasmid crosses mid-cell. Positive asymmetry corresponds to more ParA in the cell half to plasmid crosses into. **(I)** Same as **(H)**, but data were binned based on the configuration before and after a crossing event of a plasmid. The top panel includes crossing events where the absolute asymmetry in plasmid number is unchanged (e.g., from 2:1 to 1:2 or 3:2 to 2:3). The bottom panel encompasses crossing events that equalise the number of plasmids in both cell halves (e.g., from 3:1 to 2:2 or 4:2 to 3:3). **(J)** ParA asymmetry is binned by equal (the same number of plasmids in both cell halves) and unequal plasmid partitioning (different number of plasmids in both halves). For unequal partitioning, positive asymmetry values correspond to more plasmids in the cell half with less ParA (as indicated on the left violin plot). **(K)** Cartoon depicting the order of events. **(G)-(J)** considers only crossing events after the onset of nucleoid constriction. **(B)** and **(G)-(I)** were generated using 5219 cell cycles grown on M9-Glycerol.

This sequence of events is conceptually similar to the membrane oscillations of the ParA-like protein MinD between the *E. coli* cell poles. These oscillations occur due to the recruitment of MinE, which stimulates MinD hydrolysis and dissociates it from the membrane. To explore this connection further, we analysed how the asymmetry in the ParB signal itself (ParB-mTurquoise2), rather than plasmid number, correlates temporally to ParA asymmetry. For each cell cycle, we can then detect whether ParA recruits its own inhibitor ParB (akin to MinD recruiting MinE) as suggested by the

population-level analysis above against the alternative that ParB recruits and is displaced by ParA. We did this by measuring whether the temporal curve of ParB asymmetry vs ParA asymmetry rotates clockwise or anticlockwise (Figure S6A,B). We found that it primarily rotates anti-clockwise indicating that ParA recruits and is displaced by ParB (Figure S6C-E). This is consistent with the current understanding of the system: ParB-coated plasmids (more precisely, the partition complex) move up the gradient of nucleoid-associated ParA-ATP, all the while dissociating ParA-ATP through stimulation of ATP hydrolysis.

Cooperative DNA-binding explains ParA flipping

Based on our results thus far, we suggest the following explanation for ParA flipping. In cells with a constricted nucleoid, the unequal partitioning of ParB, primarily through the unequal partitioning of plasmids, results in different overall ParB-induced hydrolysis rates on each nucleoid lobe. This leads to the dissociation of ParA from the lobe with more plasmids and its accumulation on the lobe with fewer. The constriction acts to insulate the two lobes by reducing the diffusion of nucleoid-associated ParA dimers between them (Surovtsev et al., 2016b; Vecchiarelli et al., 2013). Notwithstanding any heterogeneity of the ParA distribution on each lobe, the asymmetry between the two cell halves tends to result in a sharp, almost step-like gradient of ParA across the constriction, or equivalently a strong directed flux of ParA across mid-cell (Figure S7). We speculate that this flux directs the movement of a midcell-proximal plasmid from the nucleoid lobe with more plasmids and less ParA to the lobe with fewer plasmids and more ParA through, as has been proposed, the formation of ParA-ParB protein tethers connecting the plasmid to the underlying nucleoid (Hu et al., 2017; Köhler et al., 2022; Surovtsev et al., 2016a).

However, to our knowledge, none of the existing models of the ParABS system, including our own, display ParA oscillations (flips) of the type described here. Rather, if and when they occur, ParA oscillations are concomitant with oscillatory movement of (all of) the plasmids and are not demarcated by the midcell (Köhler et al., 2022; Surovtsev et al., 2016a). In our experiments, we see the majority of plasmids in the cell apparently unaffected by the often extreme difference in ParA levels in each cell half with plasmids remaining regularly positioned within each nucleoid. As described above only the movement of a plasmid across the mid-cell appears to correlate with ParA oscillations (flipping). This indicates that some ingredient is missing from the current models.

The bistable nature of the ParA profile (in particular that ParA can be asymmetric even when plasmids are equally partitioned as in Figure 3E,F) suggests cooperativity may be involved. Indeed, the ParA of the P1 plasmid, *Thermus thermophilus* and *V. Cholerae* have been shown to bind non-specific DNA cooperatively (Baxter et al., 2020; Leonard et al., 2005; Parker et al., 2021; Chodha et al., 2023). Importantly, while oligomerization appears to be involved, it is evidently transient as ParA associates uniformly to and from the DNA (Chodha et al., 2023; Hwang et al., 2013; Vecchiarelli et al., 2013, 2010). Cooperative binding, albeit to the membrane, also occurs for MinD and is considered a key requirement for pattern formation in that system (Halatek and Frey, 2012; Heermann et al., 2020; Huang et al., 2003). We therefore studied the effect of cooperative ParA binding on the system by implementing it into our previous model 'Hopping and relay' model (Köhler et al., 2022). Note that we do not specify the molecular details of the cooperativity i.e. whether bound ParA recruit unbound ParA directly or indirectly e.g. by stimulating the transition of cytosolic dimers to their DNA-binding-competent state (Chodha et al., 2023; Vecchiarelli et al., 2010).

Independent of the exact mechanism, cooperative ParA binding creates a positive feedback loop in which more ParA is recruited to the location where already bound ParA is greatest, namely furthest from any plasmids (Figure 4A,B). This higher concentration, in turn, recruits more ParA, further amplifying the asymmetry (Figure 4B). In our simulations, this indeed produced an asymmetric ParA distribution and flips not dissimilar to our experimental observation (Figure 4D, ii). However, the asymmetry was relatively weak and there was little effect on the plasmids, which remained equally positioned across the cell and in particular the middle plasmid (of three) was maintained at mid-cell in contrast to what we observe experimentally post-constriction (Figure 2E).

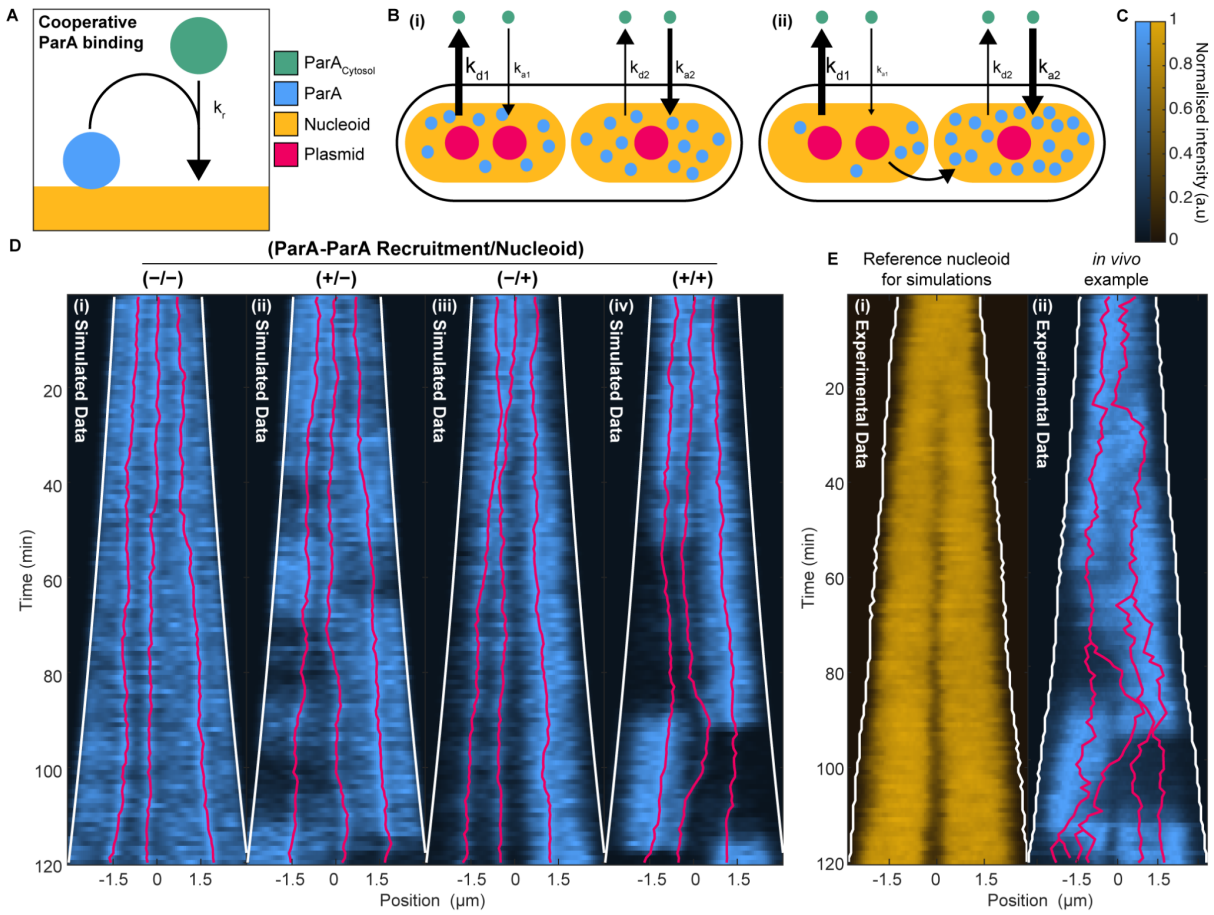

Figure 4. Cooperative ParA binding leads to robust ParA migration. **(A)** A cartoon of nucleoid-bound ParA cooperatively recruiting cytosolic ParA. **(B)** A cartoon of plasmid-induced ParA migration in a cell with two nucleoids. **(i)** Plasmid-bound ParB stimulates ParA hydrolysis, therefore increasing the rate of ParA dissociation from the nucleoid. The nucleoid with more plasmids has a higher net dissociation rate (k_{d1}) than the other nucleoid (k_{d2}) and therefore contains less nucleoid-bound ParA. **(ii)** The difference in ParA is further increased by cooperative ParA binding. Once the majority of ParA is bound to the nucleoid with fewer plasmids, the mid-cell proximal plasmid on the other nucleoid is attracted by ParA and moves towards the other nucleoid. **(C)** Colour scales for **(D)** & **(E)**. **(D)** Simulations were performed under four conditions: without any modifications **(i)**, with the incorporation of ParA cooperativity **(ii)**, with the inclusion of a nucleoid model **(iii)**, and with both ParA cooperativity and the nucleoid model **(iv)**. **(E)** Experimental kymographs of the nucleoid **(i)** and ParA **(ii)** signal from example cell cycles. Plasmid positions are overlaid in red. The nucleoid signal of this cell is used to implement the nucleoid in the simulations shown in **(D, iii & iv)**. See Figure S8 and methods for details of the parameters used in the simulations.

Reasoning that nucleoid constriction is important for both the ParA asymmetry and the exclusion of plasmids from mid-cell (as observed post-constriction), we incorporated the nucleoid itself into our simulations using the actual HU-mCherry profile from a representative cell (Figure 4E, i) (see

methods for details). First, we examined nucleoid constriction without cooperative binding and found that after constriction the plasmids separate to each nucleoid lobe with ParA (Figure 4D, iii). However, this configuration was maintained until the end of the cell cycle and no ParA flips or plasmid crossing events and mostly weak ParA asymmetry were observed. On the other hand, when we included both nucleoid constriction and cooperative ParA binding, we found strong ParA asymmetry, the greatest of the three cases, and more realistic plasmid dynamics (Figure 4D, iv). The middle plasmid stochastically (i.e. could take some time to begin) moves up the sharp mid-cell gradient formed by the ParA asymmetry. Shortly afterwards, ParA flips to 'escape' from the now two plasmids in that cell half and the cycle repeats.

As noted earlier, ParA is also observed to flip even in the absence of any change in the plasmid distribution between the two cell halves (Figure 3B,E). Such 'un-induced' flips mostly occurred when plasmids were equally distributed between cell halves (71% of the cases). To test if our model could reproduce this behaviour we also simulated cells with four plasmids (Figure S9). Firstly, we found that nucleoid constriction on its own could not generate an asymmetric ParA distribution when the plasmids were equally partitioned, further discounting this scenario. However, in the presence of both nucleoid constriction and cooperative ParA binding, we found that ParA asymmetry and flips could occur even without a change in the plasmid distribution (Figure S9), consistent with our experimental observations.

To further evaluate our model, we next looked for outlier cell cycles in our data that could serve as tests to challenge the model. In particular, we looked for cell cycles that showed unusual ParA/nucleoid dynamics and identified two such patterns. The first was the transient remerging of the two nucleoids (or nucleoid lobes) of the cell (Figure 5A), which we speculate could be due to the action of the DNA repair machinery. During remerging, ParA, which is typically localised to one nucleoid beforehand, redistributes to cover the entire remerged nucleoid, before becoming asymmetric again upon nucleoid re-separation. When we simulated the plasmid and ParA dynamics of these cell cycles using the measured nucleoid (HU-mCherry) signal and plasmid positions as inputs, we found that we could qualitatively reproduce the same ParA dynamics (Figure 5B).

The second unusual pattern was observed in cells grown on LB media. In this condition the onset of nucleoid constriction could occur in the previous cell cycle (Figure 2G) such that cells could have four nucleoid lobes before their division. This was most apparent and extreme in cells that divided late (Figure 5C). In these cells ParA was very often localised entirely to one of the four nucleoid lobes, typically one of the outer two. Using the measured nucleoid signal as an input, we found that our model could also reproduce this behaviour (Figure 5D).

Note however, that, like the real system, our simulations are stochastic and can therefore produce different behaviours for the same input nucleoid profile and initial plasmid positions. While we cannot rerun the same cell cycle experimentally, we can rerun our simulations. Though our simulations occasionally differed from the *in vivo* observations (e.g. to which nucleoid ParA was localised after re-splitting), they agreed qualitatively. In particular, all simulations showed ParA becoming more uniform during remerging of the nucleoid (as observed *in vivo*), though in ~25% of the simulations this was very short-lived (as shown in Figure 5B(iii)). For the case of multiple nucleoids, 65% of simulations matched the *in vivo* observation (ParA localised to one of the four nucleoids) while 35% differed by having more than one ParA-containing nucleoid at the end of the cycle.

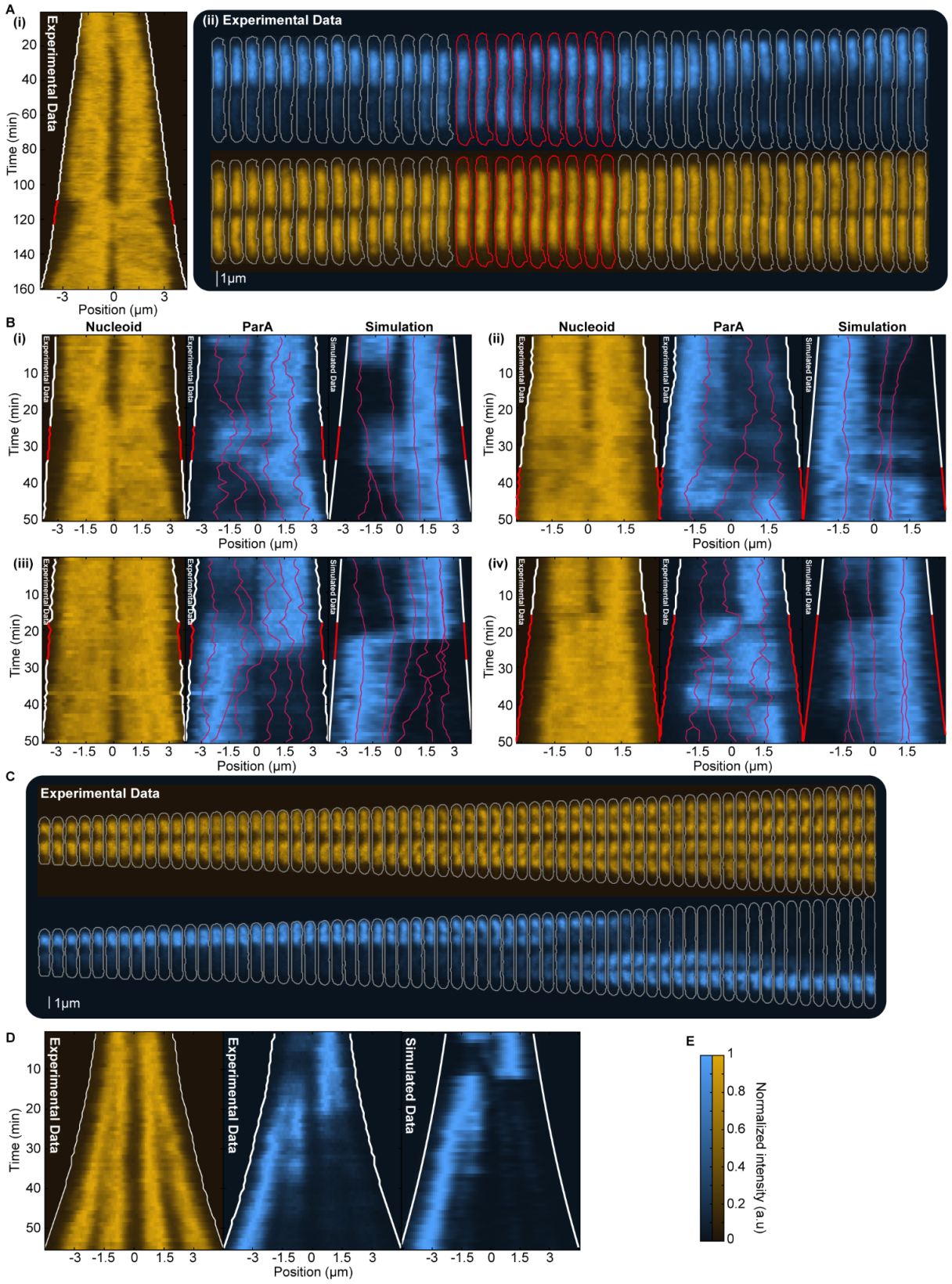

Figure 5: Atypical ParA dynamics replicated by our stochastic model. **(A)** Example of transient remerging of the nucleoid. **(i)** Kymograph of the nucleoid (HU-mCherry) of a complete cell cycle with white lines indicating the border of the cell (red when the nucleoid remerges). **(ii)** Fragment of both nucleoid (bottom) and ParA (top) signal of the same cell cycle in **(i)** centred around the remerging event (red cell outlines). **(B)** Four examples of 50 minute fragments of cell cycles in which the nucleoid remerges. Each shows the nucleoid and ParA signal of a cell cycle followed by an example simulation using the

same nucleoid profile. Plasmid trajectories are displayed as red lines. For **(iii)** 700 ParA dimers were used and 1000 for **(ii)** & **(iv)**. This was chosen to better match the experimental data. For each of **(i)** to **(iv)**, 300 simulations were performed. **(C)** A complete cell cycle grown in LB, with the nucleoid in orange and ParA in blue. This cell cycle stands out due to its abnormal size and the presence of four clearly separate nucleoids and a strongly localised ParA distribution. **(D)** Kymographs of the nucleoid and ParA signals from **(C)** and a kymograph of the simulated ParA. The simulations used the nucleoid profile, cell size, and duration from **(C)**. For cells grown on LB media we did not acquire ParB-mTurquoise2 signal therefore no plasmid trajectories are shown. The plasmid number and initial positions used in the simulations were chosen based on their expected values. **(E)** Colorbars for **(A)-(D).**

In conclusion, our model displays a remarkable ability to reproduce our experimental observations, particularly concerning the dynamics of ParA flips, both plasmid-induced and -uninduced. While there were instances where the *in vivo* and *in silico* results diverged due to the inherent stochasticity of our model, the consistency between our simulations and experimental observations was striking. This supports our hypothesis that cooperative ParA binding (alongside nucleoid constriction) is a key component for the dynamics of this system.

The Role of ParA Flips

What is the purpose of the ParA flipping? We hypothesise that it is a mechanism to ensure correct plasmid partitioning after nucleoid constriction has occurred, distinct from the previously described regular positioning of plasmids. Since F plasmids are typically found within the highest density regions of the nucleoid (presumably due to the tethering between plasmid-bound ParB and nucleoid-bound ParA) (Le Gall et al., 2016), it is likely that they would be excluded from, and have difficulty crossing, the site of nucleoid constriction simply due to the lower amount of DNA and hence ParA there. We see this in our simulations even without cooperative binding (Figure 4D, iii). As a result, once the nucleoid has constricted, positioning with each lobe is essentially no longer relevant as the plasmids of each lobe would be destined for a specific daughter cell. This challenges the current paradigm of the ParABS system as a *positioning* system. Richer growth conditions result in earlier nucleoid constriction (Figure 2F) (Govers et al., 2023). But if the nucleoid constricts early in the cell cycle then any asymmetry in the number of plasmids in each lobe will be amplified upon plasmid replication since replication events will occur more frequently in the nucleoid lobe with the most plasmids. Thus, post-nucleoid constriction *partitioning* between the nucleoid lobes is required to ensure accurate inheritance to each daughter cell. This recalls the original naming of ParABS as a *par*titioning rather than positioning system.

Our results suggest that ParA flipping is such a mechanism. Post-nucleoid constriction, a disparity in the number of plasmids in each cell half is associated with an asymmetry in ParA levels with more ParA on average in the cell half with fewer plasmids (Figure 3J). This results in a sharp ParA gradient across the constriction (Figure S7). A plasmid in the cell half with more plasmids then appears to follow, or be captured by, this gradient and move to the cell half with fewer plasmids and most ParA (Figure 3G-J). ParA then re-equilibrates, often flipping to the other cell half and the process repeats (Figure 3K). Overall this redistributes plasmids, as they are being replicated, between the two cell halves resulting in equal partitioning to the daughter cells.

To test if ParA flipping can indeed improve plasmid stability, we incorporated random plasmid replication into our stochastic simulations. Focusing first on the extreme case of cells born with a single plasmid, we found that plasmid-crossing-induced flipping of ParA due to cooperative ParA binding improved plasmid partitioning and hence stability (Figure 6A). Without cooperative binding, plasmids were not always redistributed between the two cell halves, especially when replication

occurred after the onset of nucleoid constriction, and ParA was simply maintained in the cell half with fewer plasmids. As a result, plasmid loss could easily occur.

To quantify the effect of this on plasmid stability within a population, we performed simulations of plasmid positioning over multiple generations, each new generation maintaining a random subset of the produced daughters of the previous generation. The initial plasmid copy number distribution was taken from our experimental data as were the timings of plasmid replication (see the materials and methods for details). We then measured the fraction of simulated cells with no plasmids at the end of each generation (Figure 6B). Without cooperative ParA binding, we found detectable plasmid loss when the nucleoid begins to constrict early the cell cycle, with a loss rate per generation of 6×10^{-3} for the extreme case of constriction from birth (as we observed for rich media (Figure 2F,G)). On the other hand, with cooperative binding, there were no incidences of plasmid loss across all 10,000 cell cycles simulated irrespective of the constriction timing, indicating a loss rate of at most $\sim 10^{-4}$, which is in the typical measured range (Austin and Abeles, 1983; Nordström and Austin, 1989; Sanchez et al., 2015; Tal and Paulsson, 2012). The loss rate was even higher in the absence of cooperative binding (up to 2×10^{-2}) when we used the slightly lower copy number distribution of an F plasmid variant that has only ParB labelled (Köhler et al., 2023). These findings support our hypothesis that ParA flipping is a mechanism to partition plasmids between the two lobes of the constricted nucleoid and is important for growth conditions in which nucleoid constriction occurs early in the cell cycle.

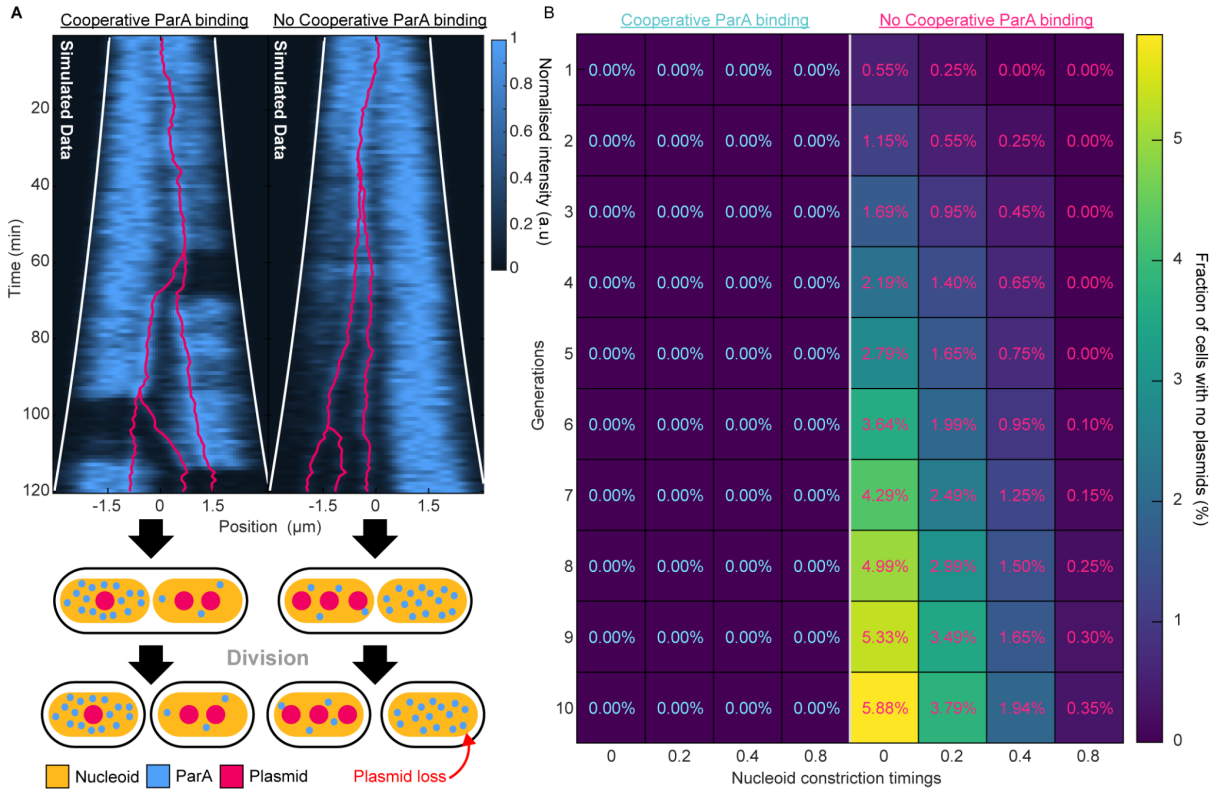

Figure 6. Cooperative ParA binding ensures plasmid stability. **(A)** (Top) Kymograph of a simulated cell with and without ParA cooperativity using the nucleoid profile shown in Figure 4E. (Bottom) Schematic representation of nucleoid, plasmids and ParA distribution before and after division for the two cases. In the non-cooperative scenario, only one cell inherits the plasmids. **(B)** ParABS system simulations were performed both with and without cooperative ParA binding across four distinct nucleoid constriction formation timings (0 birth, 1 division), spanning 10 generations. Each data point, representing

~1,000 simulated cells, indicates the fraction of cells without plasmids in a particular condition and generation. At the end of each generation, the final plasmid positions are used to ascertain the copy number at birth distribution for the subsequent generation. Plasmid replication frequency and timing are randomly chosen from our experimental data based on the initial number of plasmids within a cell. The initial distribution of plasmids for the first generation was taken from our experimental data. For all our simulations, we utilised the nucleoid profile depicted in Figure 4E, i. This was then scaled temporally to place the onset of nucleoid constriction at the given relative cell ages.

Discussion

Over the past several decades, extensive research on the ParABS system has shed light on numerous aspects of its function and role in DNA segregation, most notably the *in vitro* reconstitutions of the ParABS systems of the F and P1 plasmids (Hwang et al., 2013; Vecchiarelli et al., 2014b, 2013). Even so, surprises remained as evidenced by the recent discovery that many ParB proteins are CTPases that act like DNA clamps, loading at the *parS* sites and subsequently sliding along the DNA (Antar et al., 2021; De Asis Balaguer et al., 2021; Jalal et al., 2021, 2020; Osorio-Valeriano et al., 2021, 2019; Soh et al., 2019; Taylor et al., 2021). At the same time, techniques such as super resolution microscopy and chromatin immunoprecipitation (ChIP-Seq) have deepened our understanding of how ParA and ParB behave within cells (Debaugny et al., 2018; Guilhas et al., 2020; Ietswaart et al., 2014; Le Gall et al., 2016; Lim et al., 2014; Sanchez et al., 2015; Surovtsev et al., 2016b). However, how the *in vivo* dynamics of ParA connect with cargo positioning has remained unclear. In particular, the flipping behaviour of ParA that has been observed for the systems of plasmids F and TP228, and of *Vibrio cholerae* have not been explained (Ah-Seng et al., 2013; Chodha et al., 2023; McLeod et al., 2017). The current theory that oscillations arise from each plasmid following a self-created retracting gradient of ParA across the cell that fills in behind them (Hu et al., 2017; Jindal and Emberly, 2019; Surovtsev et al., 2016a; Walter et al., 2017) is not consistent with our *in vivo* observations in which ParA migration is demarcated by the mid-cell (Figure 1) and is only correlated to the movement of the central plasmid with the others seemingly unaffected (Figures 2 & 3). We also discovered that the localisation of ParA to one cell half, and its flipping between cell halves, occurs only after the onset of nucleoid constriction (Figure 2). Based on these observations, we propose that ParA binds to the nucleoid cooperatively and have shown here how this, along with constriction of nucleoid, can reproduce the *in vivo* behaviour. Note that while our simulations are not quantitative in the sense that there are unconstrained parameters, the fact that we can qualitatively reproduce all our measurements still provides strong support for the model.

Evidence of cooperative ParA binding to non-specific DNA has already been found for several systems including P1 plasmid, *V. cholerae* and *T. thermophilus* (Baxter et al., 2020; Chodha et al., 2023; Leonard et al., 2005; McLeod et al., 2017; Parker et al., 2021). In a similar vein, MinD, a relative of ParA, displays cooperative binding, albeit to the membrane rather than DNA (Hu et al., 2002; Lackner et al., 2003). Moreover, older *in vitro* studies showed that ParA, including from F plasmid, can form filaments (Barillà et al., 2005; Bouet et al., 2007; Ebersbach et al., 2006; Leonard et al., 2005; Lim et al., 2005). While these are not believed to occur *in vivo,* it nonetheless indicates the potential for self-interaction beyond dimer formation. Indeed, F-plasmid ParA is already known to bind cooperatively to the promoter of its *par* operon (Boudsocq et al., 2021). As for the molecular mechanism of the cooperativity, our model does not specify the details but we speculate that bound ParA-ATP dimers may promote the conformational change needed for cytosolic dimers to become competent for DNA binding (Chodha et al., 2023; Vecchiarelli et al., 2010). Understanding this would likely have relevance across the diverse family of ParABS and related systems.

ParA asymmetry and flipping between nucleoid lobes occurs only after nucleoid constriction has begun. This led us to propose that flipping constitutes a second mode of action of the ParABS system that focuses on the *partitioning* of plasmids between nucleoid lobes as distinct from their *positioning* within each lobe and before nucleoid constriction. The flips establish a sharp gradient of ParA across the constriction from the nucleoid lobe with more plasmids towards the lobe with fewer. This gradient then directs the movement of a plasmid across the constriction, thereby acting to equalise the plasmid number in each lobe. Without such a mechanism, the randomness of plasmid replication and the likely difficulty of crossing the constriction would mean that any initial disparity in plasmid number would only increase with time, leading to reduced plasmid stability. Our simulations supported this reasoning and showed a significantly higher plasmid loss rate in the absence of cooperative ParA binding, and therefore also ParA asymmetry and flipping.

An interesting consequence of ParA flipping is its asymmetric inheritance. As others have noted (Hu et al., 2021), we frequently observed that almost all ParA was inherited by one of the daughter cells, leaving the other with very low levels (Figure S2E). That the system would function in this way is surprising given that ParA is an essential component of the system and is required for accurate positioning (Le Gall et al., 2016). However, the cell half with less ParA most often contains the majority of plasmids (Figure 3J). Together with the reduced repression of the *par* operon by ParA, this likely helps in the production of new ParA. In line with this, we see cells recover their ParA levels within one or two generations.

In conclusion, this study has taken an important step toward unravelling the complexities of the ParABS system. The pivotal insight from our work is that a second mode of action of the system emerges post-nucleoid constriction to ensure the equal partitioning of plasmids between nucleoid lobes. This is orchestrated by the asymmetric localisation of ParA to, and its flipping between, the lobes of the nucleoid, which our model indicates is a consequence of cooperative ParA binding to the DNA. These findings progress our understanding of how this important system functions. While we have focused on F plasmid, our results are very likely also relevant for chromosomal ParABS systems, for which ParA flipping has also been observed (Chodha et al., 2023; Marston and Errington, 1999; Quisel et al., 1999). Our work also narrows the gap between ParA and its distant homologue, the cell division protein MinD, which also oscillates within the cell and binds cooperatively, but to the membrane. We expect that future studies will discover further commonalities within this diverse family of ATPases.

Material and Methods

Strains and growth condition

All experiments use strain DLT3125 with containing the plasmid pJYB249 (Sanchez et al., 2015), a derivative of the *E. coli* K-12 strain DLT1215 (Bouet et al., 2005) containing the mini-F plasmid derivative pJYB234. This plasmid carries a functional ParB-mTurquoise2 and ParA-mVenus fusion. Overnight cultures were grown at 37 °C in LB-Media containing 10 µg/ml thymine + 10 µg/ml chloramphenicol. For microfluidic experiments the following growth media were used: M9-Glycerol: (1x M9 salts + 0.5% glycerol + 0.2% casamino acids + 0.04 mg/mL thymine + 0.2 mg/mL leucine); M9-L-Alanine: (1x M9 salts + 0.2% L-alanine + 0.04 mg/mL thymine + 0.2 mg/mL leucine + mg/ml thiamine; LB: (LB + 0.04 mg/mL thymine).

Microfluidics

Like the original mother machine (Wang et al., 2010), our design consists of a main channel through which nutrient media flows and narrow growth-channels in which cells are trapped. However, we follow (Baltekin et al., 2017) and include (i) a small opening at the end of each growth channel (ii) a waste channel connected to that opening to allow a continuous flow of nutrients through the growth channels (iii) an inverted growth-channel that is used to remove the background from fluorescence and phase contrast. We used a silicon wafer with this design to create the mother machine. We poured a polydimethylsiloxane (PDMS) mixture composed of a ratio of 1:7 (curing agent:base) over the wafer and let it rest at low pressure in a degasser for ~30 min to remove air bubbles inside. The PDMS was then baked at 80 °C overnight (~16 h). The cured PDMS was peeled off the wafer. Before imaging, the chip is bonded to a glass slide using a plasma generator (30 s at 75 W) and subsequently baked for a further 30 min at 80 °C, while the microscope is prepared.

Microscopy

We used a Nikon Ti microscope with a 100 x/1.45 oil objective and a Hamamatsu Photonics camera for all imaging. Apart from the data shown in Figure S4 all experiments were carried out using a mother machine. Overnight cultures were inoculated into fresh media for 4 hours (2 hours for LB-condition) at 30 °C before imaging. Cells were loaded into the chip through the main channel and the chip was placed into a preheated microscope at 30 °C. The cells were constantly supplied with fresh media by pumping 2 µL/min of either of the three media that defined above, through the microfluidic chip. Cells were grown for 2 hr inside the microscope before imaging. Cells were imaged at 1 minute intervals for approximately 72 hours (M9-Glycerol) and 24 hours (M9-L-Alanine & LB). Phase contrast, RFP-signal, CFP-signal and YFP-signal were captured for the M9-Glycerol. For LB and M9-L-Alanine the CFP-signal was not captured to capture more field of views per 1 minute interval.

Image processing

Our image processing pipeline for mother-machine experiments consists of three parts: (I) preprocessing, (II) segmentation and foci finding, and (III) cell and foci tracking. While Parts I and III use custom Matlab scripts, Part II is based on SuperSegger (Stylianidou et al., 2016) (Stylianidou et al., 2016), a Matlab-based package for segmenting and tracking bacteria within microcolonies (original code is available at https://github.com/wiggins-lab/SuperSegger), that we modified to better handle high-throughput data. SuperSegger employs pre-trained neural networks to segment cells by identifying their boundaries. It comes with a pre-trained model for E. coli which worked very well with our data. Therefore there was no need to train our own neural network. SuperSegger is capable of tracking cells however the tracking did not work properly with mother-machine images and so we developed our own method. Nevertheless, acknowledging that one of the main components of our pipeline, the segmentation, uses SuperSegger we refer to the entire pipeline as MotherSegger (code is available at https://gitlab.gwdg.de/murray-group/MotherSegger).

In Part I, each frame of an acquired image stack is aligned (the offset between frames in x and y is removed). Afterwards the image stack is rotated so the growth channels are vertical. A mask of the mother machine layout is fitted to the phase contrast, using cross-correlation, to identify where the growth channels are located. Each growth channel is extracted from the image stack and the flipped inverted channel is subtracted to remove the background from both the fluorescence signal and phase contrast. The images are then segmented and fluorescent foci are identified using Supersegger.

In Part III, both foci and cells are tracked. Since cells cannot change their order inside the growth channel, they can be tracked by matching similar cell length between frames (starting from the bottom of the growth channels). Once individual cell cycles are identified, the foci positions found by Supersegger are re-specified relative to the bounding box of the cell (the smallest rectangular image containing the cell mask) on each frame. Since cells are vertical in the channels without any significant tilting, the bounding box is aligned with the cell

axes. Within each cell cycle, foci are tracked between frames by finding the closest focus on the next frame inside the same cell cycle. The effect of growth on foci position was neglectable since cells grew on average much less than one pixel per frame at the 1 min frame rate and 100 min doubling time used here. Finally, half the cell length was subtracted from the foci positions along the long cell axis (vertical direction) so that 0 corresponds to the middle of the cell. The sign of the positions was also adjusted so that negative positions refer to the old-pole proximal side of the cell.

To filter out potential segmentation errors, cell cycles that do not have exactly 1 parent and 2 daughters are excluded from analysis along with their immediate relatives (with the exception of those who are pushed out of the growth channel). For the analysis of foci trajectories, we considered only trajectories coming from at least 12 consecutive frames with the same number of foci. For pB171, we used (unmodified) SuperSegger to process images of cells growing on agarose pads.

Foci were tracked using ★Track (https://gitlab.gwdg.de/murray-group/StarTrack) (Köhler et al., 2023).

Model

Our model is an extension of the previous DNA-relay model (Surovtsev et al., 2016a) that incorporates a reference nucleoid, diffusion on the nucleoid (hopping), cell growth, basal hydrolysis and cooperative binding of ParA and uses analytic expressions for the fluctuations rather than a second order approximation. Like the DNA relay model it is a 2D off-lattice stochastic model and updates positions in discrete time steps dt. The implementation was written in C++ (code is available at https://gitlab.gwdg.de/murray-group/hopping_and_relay). It operates as follows. ParA associates to the DNA non-specifically in its ATP-dependent dimer state with the rate k_a or through cooperative binding with the rate k_r. Cooperative ParA binding is implemented as such: Each nucleoid bound ParA recruits, with $k_c = k_{c0} n_{ParA-cytosol}$, a cytosolic ParA to the same position on the nucleoid. Once associated, ParA (i.e. ParA-ATP dimers) moves in two distinct ways: (i) Diffusive motion on the nucleoid with the diffusion coefficient D_h. This is an effective description of the movement of dimers due to transient unbinding events that allow them to 'hop' between DNA-strands. (ii) Between hopping events, each bound ParA dimer experiences the elastic fluctuations of the DNA strand it is bound to. This is implemented as elastic (spring-like) fluctuations around its initial position. Dimers dissociate from the nucleoid due to either basal ATP hydrolyse at a rate k_d or due to hydrolysis stimulated by ParB on the plasmid. The latter is modelled as a ParB-coated disc and ParB-ParA tethers form whenever the disk comes in contact with a ParA dimer. ParB-stimulated hydrolysis then breaks these tethers at a rate k_h, returning ParA to the cytosolic pool. The plasmid experiences the elastic force of every tethered ParA and moves according the its intrinsic diffusion coefficient D_p and the resultant force of all tethers.

As in the DNA relay model we have made some simplifications that we next make explicit. First, we only modelled three states of ParA: 'nucleoid associated' and 'cytosolic' and 'tethered'. Second, cytosolic ParA are assumed to be well mixed. This is justified based on the slow conformation changes needed to return it to a state competent for DNA-binding (Vecchiarelli et al., 2010). Third, no individual ParB molecules were modelled, rather the plasmid is treated as a disk coated with enough ParB that each nucleoid-bound ParA that makes contact with the plasmid instantaneously finds a ParB partner, therefore removing the need to model individual ParB. This is justified by the substantially higher local concentration of ParB compared to ParA at the plasmid.

The cell is modelled as a rectangle with the dimensions $L \times W$ and the nucleoid is assumed to be uniform unless a reference nucleoid is provided. The cell grows at the rate k_g each step of the simulation and all particles (ParA & Plasmid) are repositioned such that their relative position within the cell stays the same. Afterwards, the positions of ParA and the plasmid(s), are updated as follows. Between hopping events, each nucleoid associated ParA dimer fluctuates about a home position x_h. The new position $x(t + dt)$ of each dimer is given

by $x(t + dt) = x_h + \delta x$, where δx is drawn with probability $p(\delta x, dt \mid x(t) - x_h)$ where x(t) is its original position (see section 'Over-damped spring') and the normalised spring constant ($f/k_B T$ above) along each dimension is $1/\sigma_{x,y}^2$ and the diffusion coefficient D_A. During hopping events $x(t)$ and x_h are both offset by a value drawn from a Gaussian distribution with $\mu = 0$ and $\sigma = \sqrt{2D_h dt}$ for both dimensions. The displacement of the plasmid is determined similar to each ParA dimer but according to the resultant force acting on it. This resultant force vector has an effective spring constant equal to the spring constant of a single tether times the number of tethers and acts towards an equilibrium position $x_p(t) + \sum_{tethers} (x_h - x(t))/n$, where $x_p(t)$ is the plasmid position and the sum is over all (n) tethers. We ignore the effects of Torque. The intrinsic diffusion coefficient of the plasmid is D_p. If the plasmid has no tethers attached then it moves by normal diffusion, with displacements drawn from a Gaussian distribution with $\mu = 0$ and $\sigma = \sqrt{2D_p dt}$. The x and y components of all positions are updated independently and all simulations in this paper were run until the system reached equilibrium before acquiring data used for analysis.

If a reference nucleoid is defined it is resized to the same size of the cell and it is then used as a field that influences the hopping of ParA on the nucleoid. It uses the second order approximation (Branka and Heyes, 1988) in combination with the effector factor p_n to bias the movement of the ParA towards the greatest density of the nucleoid.

Kymographs and Normalisation

Kymographs visually represent cellular dynamics across time. Single cell kymographs of an individual cell cycle (e.g. Figure 1A) are a stack of line profiles generated by averaging the signal across the cell's short axis on each frame. To ensure consistent visibility of the signal throughout the cell cycle, regardless of any increase or decrease in the actual signal, each line profile was normalised by dividing by its maximum value. Averaged Kymographs combine line profiles across multiple cell cycles. Before combining, the line profiles were normalised in the same way. We show two distinct types of averaged kymographs. (1) Figure 1D: This average kymograph illustrates the mean ParA signal, synchronised by the migration of ParA from one cell half to the other. To achieve this alignment, all line profiles were normalised to span from -1 to 1. (2) Figure 2F: This illustrates average kymographs, combining all line profiles of the nucleoid from every cell cycle, grouped by growth condition. Here, we employed a two-step normalisation procedure. Time Normalisation: Every cell cycle starts at 0 (birth) and proceeds to 1 (division). Length Normalisation: At birth, each cell has a standardised length of 1, growing to 2 at division, with the length of time points in between adjusted to reflect exponential growth. Lastly, when displaying single-cell kymographs of ParA of simulated cells, the ParA location distribution is subjected to Gaussian blurring. This is done to replicate the point spread function inherent to microscopy.

Simulations for Plasmid Stability

This section details how simulations were conducted to ascertain plasmid loss (Figure 6B). Simulations were conducted across four unique nucleoid constriction formation timings (0 birth, 1 division) over a course of 10 generations. Each data point comprises data from at least 1000 simulated cell cycles, each lasting 120 minutes and starting with the average newborn cell length of 3 µm. The initial distribution of plasmids for generation 1 was derived from our experimental glycerol growth condition data. At the end of each simulated cell cycle, plasmid inheritance by the offspring was determined based on the number of plasmids in each cell half. This defined the distribution of plasmid numbers at birth for the next generation. This distribution is then multiplied by 1000 to determine the number of cells starting with a specific number of plasmids at birth (non-integer

numbers are rounded up). To emulate plasmid replication, we relied on our experimental data. For every real cell cycle, plasmid replication timings in terms of relative cell age were determined. Each simulated cell was then assigned a random set of relative replication timings from the experimental pool, with the only condition being that the initial number of plasmids at birth matched. Every simulation used the nucleoid profile portrayed in Figure 4E, i, scaled temporally to align the onset of nucleoid constriction with the specified relative cell ages.

To calculate the loss rate the following function is used: $P_{loss} = \sqrt[10]{1 - f_{loss}}$, where f_{loss} is the fraction of cells which lost the plasmid.

References

Ah-Seng Y, Rech J, Lane D, Bouet J-Y. 2013. Defining the Role of ATP Hydrolysis in Mitotic Segregation of Bacterial Plasmids. *PLoS Genet* **9**:e1003956. doi:10.1371/journal.pgen.1003956

Antar H, Soh Y-M, Zamuer S, Bock FP, Anchimiuk A, De Los Rios P, Gruber S. 2021. Relief of ParB autoinhibition by parS DNA catalysis and ParB recycling by CTP hydrolysis promote bacterial centromere assembly. *Sci Adv* **7**:eabj2854. doi:10.1126/sciadv.abj2854

Austin S, Abeles A. 1983. Partition of unit-copy miniplasmids to daughter cells: I. P1 and F miniplasmids contain discrete, interchangeable sequences sufficient to promote equipartition. *J Mol Biol* **169**:353–372. doi:10.1016/S0022-2836(83)80055-2

Baltekin Ö, Boucharin A, Tano E, Andersson DI, Elf J. 2017. Antibiotic susceptibility testing in less than 30 min using direct single-cell imaging. *Proc Natl Acad Sci* **114**:9170–9175. doi:10.1073/pnas.1708558114

Barillà D, Rosenberg MF, Nobbmann U, Hayes F. 2005. Bacterial DNA segregation dynamics mediated by the polymerizing protein ParF. *EMBO J* **24**:1453–64. doi:10.1038/sj.emboj.7600619

Baxter JC, Waples WG, Funnell BE. 2020. Nonspecific DNA binding by P1 ParA determines the distribution of plasmid partition and repressor activities. *J Biol Chem* **295**:17298–17309. doi:10.1074/jbc.RA120.015642

Boudsocq F, Salhi M, Barbe S, Bouet J-Y. 2021. Three ParA Dimers Cooperatively Assemble on Type Ia Partition Promoters. *Genes* **12**:1345. doi:10.3390/genes12091345

Bouet J-Y, Ah-Seng Y, Benmeradi N, Lane D. 2007. Polymerization of SopA partition ATPase: regulation by DNA binding and SopB. *Mol Microbiol* **63**:468–481. doi:10.1111/j.1365-2958.2006.05537.x

Branka AC, Heyes DM. 1988. Algorithms for Brownian dynamics simulation. *Phys Rev E* **58**:2611--2615. doi:10.1103/PhysRevE.58.2611

Chodha SS, Brooks AC, Davis PJ, Ramachandran R, Chattoraj DK, Hwang LC. 2023. Kinetic principles of ParA2-ATP cycling guide dynamic subcellular localizations in Vibrio cholerae. *Nucleic Acids Res* gkad321. doi:10.1093/nar/gkad321

De Asis Balaguer F, Aicart-Ramos C, Lm Fisher G, De Bragança S, Pastrana CL, Dillingham MS, Moreno-Herrero F. 2021. Cytidine triphosphate promotes efficient ParB-dependent DNA condensation by facilitating one-dimensional spreading from parS. *eLife* 2021.02.11.430778. doi:10.7554/eLife.67554

Debaugny RE, Sanchez A, Rech J, Labourdette D, Dorignac J, Geniet F, Palmeri J, Parmeggiani A, Boudsocq F, Anton Leberre V, Walter J-C, Bouet J-Y. 2018. A conserved mechanism drives partition complex assembly on bacterial chromosomes and plasmids. *Mol Syst Biol* **14**:8516. doi:10.15252/msb.20188516

Ebersbach G, Gerdes K. 2001. The double par locus of virulence factor pB171: DNA segregation is correlated with oscillation of ParA. *Proc Natl Acad Sci U S A* **98**:15078–83. doi:10.1073/pnas.261569598

Ebersbach G, Ringgaard S, Moller-Jensen J, Wang Q, Sherratt DJ, Gerdes K. 2006. Regular

cellular distribution of plasmids by oscillating and filament-forming ParA ATPase of plasmid pB171. *Mol Microbiol* **61**:1428–1442. doi:10.1111/j.1365-2958.2006.05322.x
Gerdes K, Moller-Jensen J, Jensen RB. 2000. Plasmid and chromosome partitioning: Surprises from phylogeny. *Mol Microbiol* **37**:455–466. doi:10.1046/j.1365-2958.2000.01975.x
Govers SK, Campos M, Tyagi B, Laloux G, Jacobs-Wagner C. 2023. Apparent simplicity and emergent robustness in bacterial cell cycle control. doi:10.1101/2023.01.16.524295
Guilhas B, Walter J-C, Rech J, David G, Walliser NO, Palmeri J, Mathieu-Demaziere C, Parmeggiani A, Bouet J-Y, Le Gall A, Nollmann M. 2020. ATP-Driven Separation of Liquid Phase Condensates in Bacteria. *Mol Cell* **79**:293-303.e4. doi:10.1016/j.molcel.2020.06.034
Halatek J, Frey E. 2012. Highly Canalized MinD Transfer and MinE Sequestration Explain the Origin of Robust MinCDE-Protein Dynamics. *Cell Rep* **1**:741–752. doi:10.1016/j.celrep.2012.04.005
Hatano T, Niki H. 2010. Partitioning of P1 plasmids by gradual distribution of the ATPase ParA. *Mol Microbiol* **78**:1182–1198. doi:10.1111/j.1365-2958.2010.07398.x
Hatano T, Yamaichi Y, Niki H. 2007. Oscillating focus of SopA associated with filamentous structure guides partitioning of F plasmid. *Mol Microbiol* **64**:1198–1213. doi:10.1111/j.1365-2958.2007.05728.x
Heermann T, Ramm B, Glaser S, Schwille P. 2020. Local Self-Enhancement of MinD Membrane Binding in Min Protein Pattern Formation. *J Mol Biol* **432**:3191–3204. doi:10.1016/j.jmb.2020.03.012
Hester CM, Lutkenhaus J. 2007. Soj (ParA) DNA binding is mediated by conserved arginines and is essential for plasmid segregation. *Proc Natl Acad Sci* **104**:20326–20331. doi:10.1073/pnas.0705196105
Hirano M, Mori H, Onogi T, Yamazoe M, Niki H, Ogura T, Hiraga S. 1998. Autoregulation of the partition genes of the mini-F plasmid and the intracellular localization of their products in Escherichia coli. *Mol Gen Genet MGG* **257**:392–403. doi:10.1007/s004380050663
Hu L, Rech J, Bouet J-Y, Liu J. 2021. Spatial control over near-critical-point operation ensures fidelity of ParABS-mediated DNA partition. *Biophys J* **120**:3911–3924. doi:10.1016/j.bpj.2021.08.022
Hu L, Vecchiarelli AG, Mizuuchi K, Neuman KC, Liu J. 2017. Brownian Ratchet Mechanism for Faithful Segregation of Low-Copy-Number Plasmids. *Biophys J* **112**:1489–1502. doi:10.1016/j.bpj.2017.02.039
Hu L, Vecchiarelli AG, Mizuuchi K, Neuman KC, Liu J. 2015. Directed and persistent movement arises from mechanochemistry of the ParA/ParB system. *Proc Natl Acad Sci* **112**:E7055–E7064. doi:10.1073/pnas.1505147112
Hu Z, Gogol EP, Lutkenhaus J. 2002. Dynamic assembly of MinD on phospholipid vesicles regulated by ATP and MinE. *Proc Natl Acad Sci* **99**:6761–6766. doi:10.1073/pnas.102059099
Huang KC, Meir Y, Wingreen NS. 2003. Dynamic structures in Escherichia coli: Spontaneous formation of MinE rings and MinD polar zones. *Proc Natl Acad Sci* **100**:12724–12728. doi:10.1073/pnas.2135445100
Hwang LC, Vecchiarelli AG, Han Y-W, Mizuuchi M, Harada Y, Funnell BE, Mizuuchi K. 2013. ParA-mediated plasmid partition driven by protein pattern self-organization. *EMBO J* **32**:1238–1249. doi:10.1038/emboj.2013.34
Ietswaart R, Szardenings F, Gerdes K, Howard M. 2014. Competing ParA structures space bacterial plasmids equally over the nucleoid. *PLoS Comput Biol* **10**:e1004009. doi:10.1371/journal.pcbi.1004009
Jalal AS, Tran NT, Le TBK. 2020. ParB spreading on DNA requires cytidine triphosphate in vitro. *eLife* **9**. doi:10.7554/eLife.53515
Jalal AS, Tran NT, Stevenson CE, Chimthanawala A, Badrinarayanan A, Lawson DM, Le TB. 2021. A CTP-dependent gating mechanism enables ParB spreading on DNA. *eLife* **10**:e69676. doi:10.7554/eLife.69676

Jindal L, Emberly E. 2019. DNA segregation under Par protein control. *PLOS ONE* **14**:e0218520. doi:10.1371/journal.pone.0218520
Köhler R, Kaganovitch E, Murray SM. 2022. High-throughput imaging and quantitative analysis uncovers the nature of plasmid positioning by ParABS. *eLife* **11**:e78743. doi:10.7554/eLife.78743
Köhler R, Sadhir I, Murray SM. 2023. ★Track: Inferred counting and tracking of replicating DNA loci. *Biophys J* **122**:1577–1585. doi:10.1016/j.bpj.2023.03.033
Lackner LL, Raskin DM, de Boer PAJ. 2003. ATP-Dependent Interactions between Escherichia coli Min Proteins and the Phospholipid Membrane In Vitro. *J Bacteriol* **185**:735–749. doi:10.1128/jb.185.3.735-749.2003
Le Gall A, Cattoni DI, Guilhas B, Mathieu-Demazière C, Oudjedi L, Fiche J-B, Rech J, Abrahamsson S, Murray H, Bouet J-Y, Nollmann M. 2016. Bacterial partition complexes segregate within the volume of the nucleoid. *Nat Commun* **7**:12107. doi:10.1038/ncomms12107
Leonard TA, Butler PJ, Löwe J. 2005. Bacterial chromosome segregation: structure and DNA binding of the Soj dimer — a conserved biological switch. *EMBO J* **24**:270–282.
Lim GE, Derman AI, Pogliano J. 2005. Bacterial DNA segregation by dynamic SopA polymers. *Proc Natl Acad Sci U S A* **102**:17658–63. doi:10.1073/pnas.0507222102
Lim HC, Surovtsev IV, Beltran BG, Huang F, Bewersdorf J, Jacobs-Wagner C. 2014. Evidence for a DNA-relay mechanism in ParABS-mediated chromosome segregation. *eLife* **3**. doi:10.7554/eLife.02758
Marston AL, Errington J. 1999. Dynamic Movement of the ParA-like Soj Protein of B. subtilis and Its Dual Role in Nucleoid Organization and Developmental Regulation. *Mol Cell* **4**:673–682. doi:10.1016/S1097-2765(00)80378-0
McLeod BN, Allison-Gamble GE, Barge MT, Tonthat NK, Schumacher MA, Hayes F, Barillà D. 2017. A three-dimensional ParF meshwork assembles through the nucleoid to mediate plasmid segregation. *Nucleic Acids Res* **45**. doi:10.1093/nar/gkw1302
Mishra D, Srinivasan R. 2022. Catching a Walker in the Act—DNA Partitioning by ParA Family of Proteins. *Front Microbiol* **13**.
Nordström K, Austin SJ. 1989. Mechanisms That Contribute to the Stable Segregation of Plasmids. *Annu Rev Genet* **23**:37–69. doi:10.1146/annurev.ge.23.120189.000345
Osorio-Valeriano M, Altegoer F, Das CK, Steinchen W, Panis G, Connolley L, Giacomelli G, Feddersen H, Corrales-Guerrero L, Giammarinaro PI, Hanßmann J, Bramkamp M, Viollier PH, Murray S, Schäfer LV, Bange G, Thanbichler M. 2021. The CTPase activity of ParB determines the size and dynamics of prokaryotic DNA partition complexes. *Mol Cell* **81**:1–16. doi:10.1016/j.molcel.2021.09.004
Osorio-Valeriano M, Altegoer F, Steinchen W, Urban S, Liu Y, Bange G, Thanbichler M. 2019. ParB-type DNA Segregation Proteins Are CTP-Dependent Molecular Switches. *Cell* **179**:1512-1524.e15. doi:10.1016/j.cell.2019.11.015
Parker AV, Mann D, Tzokov SB, Hwang LC, Bergeron JRC. 2021. The structure of the bacterial DNA segregation ATPase filament reveals the conformational plasticity of ParA upon DNA binding. *Nat Commun* **12**:5166. doi:10.1038/s41467-021-25429-2
Quisel JD, Lin DC-H, Grossman AD. 1999. Control of Development by Altered Localization of a Transcription Factor in B. subtilis. *Mol Cell* **4**:665–672. doi:10.1016/S1097-2765(00)80377-9
Ringgaard S, van Zon J, Howard M, Gerdes K. 2009. Movement and equipositioning of plasmids by ParA filament disassembly. *Proc Natl Acad Sci* **106**:19369–19374. doi:10.1073/pnas.0908347106
Rodionov O, ŁObocka M, Yarmolinsky M. 1999. Silencing of genes flanking the P1 plasmid centromere. *Science* **283**:546–549. doi:10.1126/science.283.5401.546
Sanchez A, Cattoni DI, Walter J-C, Rech J, Parmeggiani A, Nollmann M, Bouet J-Y. 2015. Stochastic Self-Assembly of ParB Proteins Builds the Bacterial DNA Segregation Apparatus. *Cell Syst* **1**:163–173. doi:10.1016/j.cels.2015.07.013
Sengupta M, Nielsen HJ, Youngren B, Austin S. 2010. P1 Plasmid Segregation: Accurate Redistribution by Dynamic Plasmid Pairing and Separation. *J Bacteriol*

192:1175–1183. doi:10.1128/JB.01245-09
Soh Y-M, Davidson IF, Zamuner S, Basquin J, Bock FP, Taschner M, Veening J-W, De Los Rios P, Peters J-M, Gruber S. 2019. Self-organization of parS centromeres by the ParB CTP hydrolase. *Science* **366**:1129–1133. doi:10.1126/science.aay3965
Stylianidou S, Brennan C, Nissen SB, Kuwada NJ, Wiggins PA. 2016. SuperSegger: robust image segmentation, analysis and lineage tracking of bacterial cells: Robust segmentation and analysis of bacteria. *Mol Microbiol* **102**:690–700. doi:10.1111/mmi.13486
Sugawara T, Kaneko K. 2011. Chemophoresis as a driving force for intracellular organization: Theory and application to plasmid partitioning. *Biophysics* **7**:77–88. doi:10.2142/biophysics.7.77
Surovtsev I, Campos M, Jacobs-wagner C. 2016a. DNA-relay mechanism is sufficient to explain ParA-dependent intracellular transport and patterning of single and multiple cargos. *Proc Natl Acad Sci* E7268–E7276. doi:10.1073/pnas.1616118113
Surovtsev I, Lim HC, Jacobs-Wagner C. 2016b. The Slow Mobility of the ParA Partitioning Protein Underlies Its Steady-State Patterning in Caulobacter. *Biophys J* **110**:2790–2799. doi:10.1016/j.bpj.2016.05.014
Tal S, Paulsson J. 2012. Evaluating quantitative methods for measuring plasmid copy numbers in single cells. *Plasmid*, A Special Issue on Chromosome Dynamics in Memory of Prof. Kurt Nordstrom **67**:167–173. doi:10.1016/j.plasmid.2012.01.004
Taylor JA, Seol Y, Budhathoki J, Neuman KC, Mizuuchi K. 2021. CTP and parS coordinate ParB partition complex dynamics and ParA-ATPase activation for ParABS-mediated DNA partitioning. *eLife* **10**:e65651. doi:10.7554/eLife.65651
Vecchiarelli AG, Han Y-W, Tan X, Mizuuchi M, Ghirlando R, Biertümpfel C, Funnell BE, Mizuuchi K. 2010. ATP control of dynamic P1 ParA-DNA interactions: a key role for the nucleoid in plasmid partition. *Mol Microbiol* **78**:no-no. doi:10.1111/j.1365-2958.2010.07314.x
Vecchiarelli AG, Hwang LC, Mizuuchi K. 2013. Cell-free study of F plasmid partition provides evidence for cargo transport by a diffusion-ratchet mechanism. *Proc Natl Acad Sci U S A* **110**:E1390-7. doi:10.1073/pnas.1302745110
Vecchiarelli AG, Neuman KC, Mizuuchi K. 2014a. A propagating ATPase gradient drives transport of surface-confined cellular cargo. *Proc Natl Acad Sci U S A* **111**:4880–5. doi:10.1073/pnas.1401025111
Vecchiarelli AG, Seol Y, Neuman KC, Mizuuchi K. 2014b. A moving ParA gradient on the nucleoid directs subcellular cargo transport via a chemophoresis force. *Bioarchitecture* **4**:154–159. doi:10.4161/19490992.2014.987581
Walter J-C, Dorignac J, Lorman V, Rech J, Bouet J-Y, Nollmann M, Palmeri J, Parmeggiani A, Geniet F. 2017. Surfing on Protein Waves: Proteophoresis as a Mechanism for Bacterial Genome Partitioning. *Phys Rev Lett* **119**:028101. doi:10.1103/PhysRevLett.119.028101
Wang P, Robert L, Pelletier J, Dang WL, Taddei F, Wright A, Jun S. 2010. Robust Growth of Escherichia coli. *Curr Biol* **20**:1099–1103. doi:10.1016/j.cub.2010.04.045

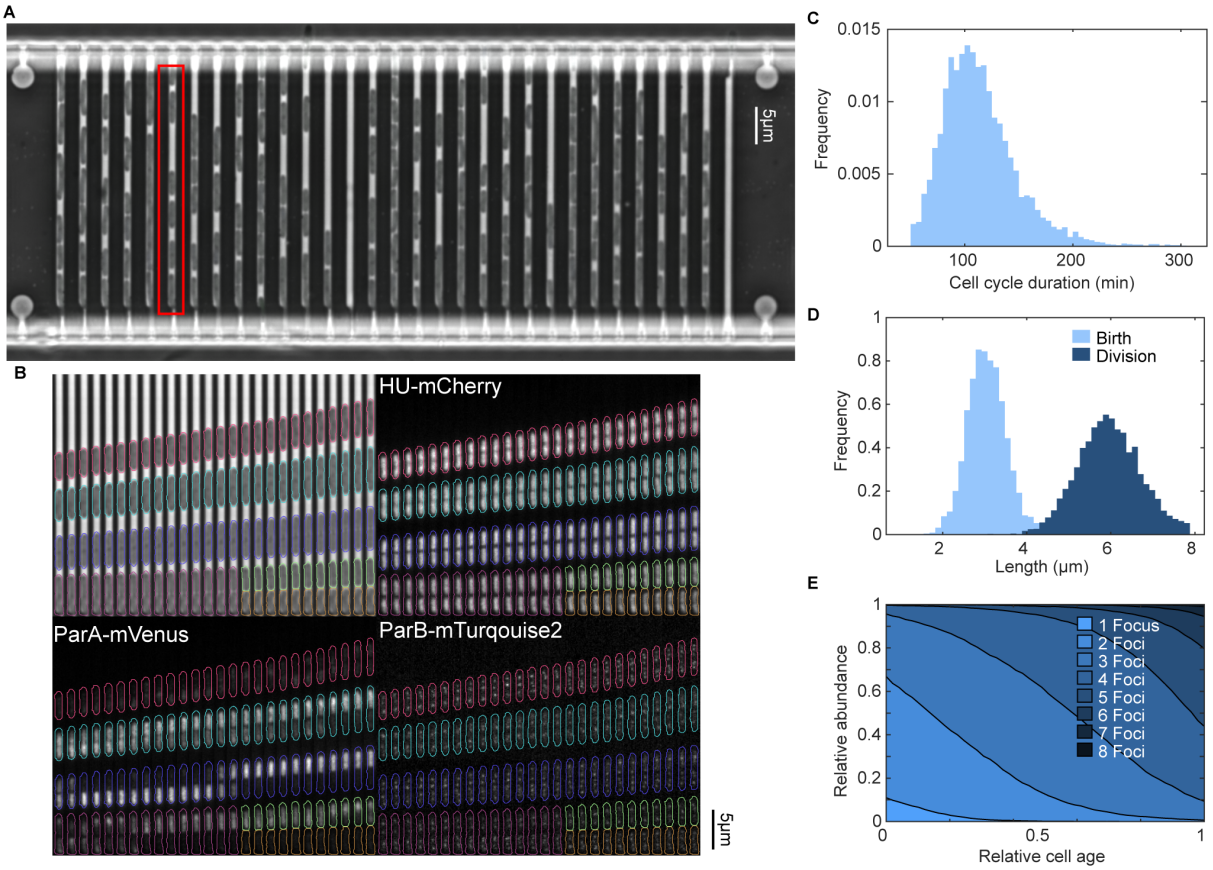

Figure S1. Overview of a mother machine experiment. **(A)** Growth channels of one field of view. **(B)** Kymograph of one growth channel of the mother machine device (The one highlighted in red in panel **(A)**). Phase contrast and 3 fluorescent channels are depicted with overlaid cell contours (same colour = same cell cycle). **(C)** Histogram of cell cycle duration of all acquired cell cycles (113.7 ± 34.8 min, mean ± SD). **(D)** Histogram of birth and division size of all acquired cell cycles. **(E)** Relative abundance of ParB foci plotted against relative cell age. The panels **(C)** to **(E)** were generated from 5219 cell cycles.

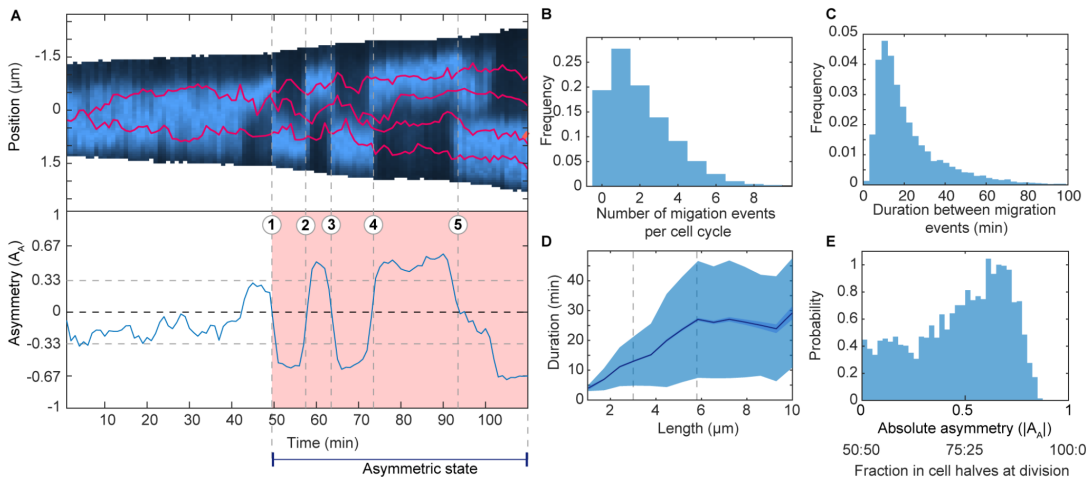

Figure S2. Properties of ParA migration patterns. **(A)** Example of the annotation of migration events (flips) and when ParA is in an asymmetric state. Top: Kymograph of ParA-mVenus signal. Red lines indicate plasmid trajectories obtained from tracking foci of ParB-mTurquoise2. Bottom: Fractional asymmetry of ParA. When the asymmetry exceeds the threshold indicated by the grey dashed lines (⅔ of the signal is localised in one cell half), the area between the zero-crossings is marked as ParA being in an asymmetric state (red shaded region). These zero-crossing points adjacent to asymmetric states (1)-(5) are defined as migration events of ParA (flips of ParA). **(B)** Distribution of the number of migration events per cell cycle. **(C)** Distribution of the duration between two flips. **(D)** The duration between migration events plotted against time since birth. **(F)** The absolute asymmetry of ParA on the last frame from each cell cycle or the fraction of ParA in both cell halves directly before division. The panels **(B)** to **(E)** were generated from 5219 cell cycles.

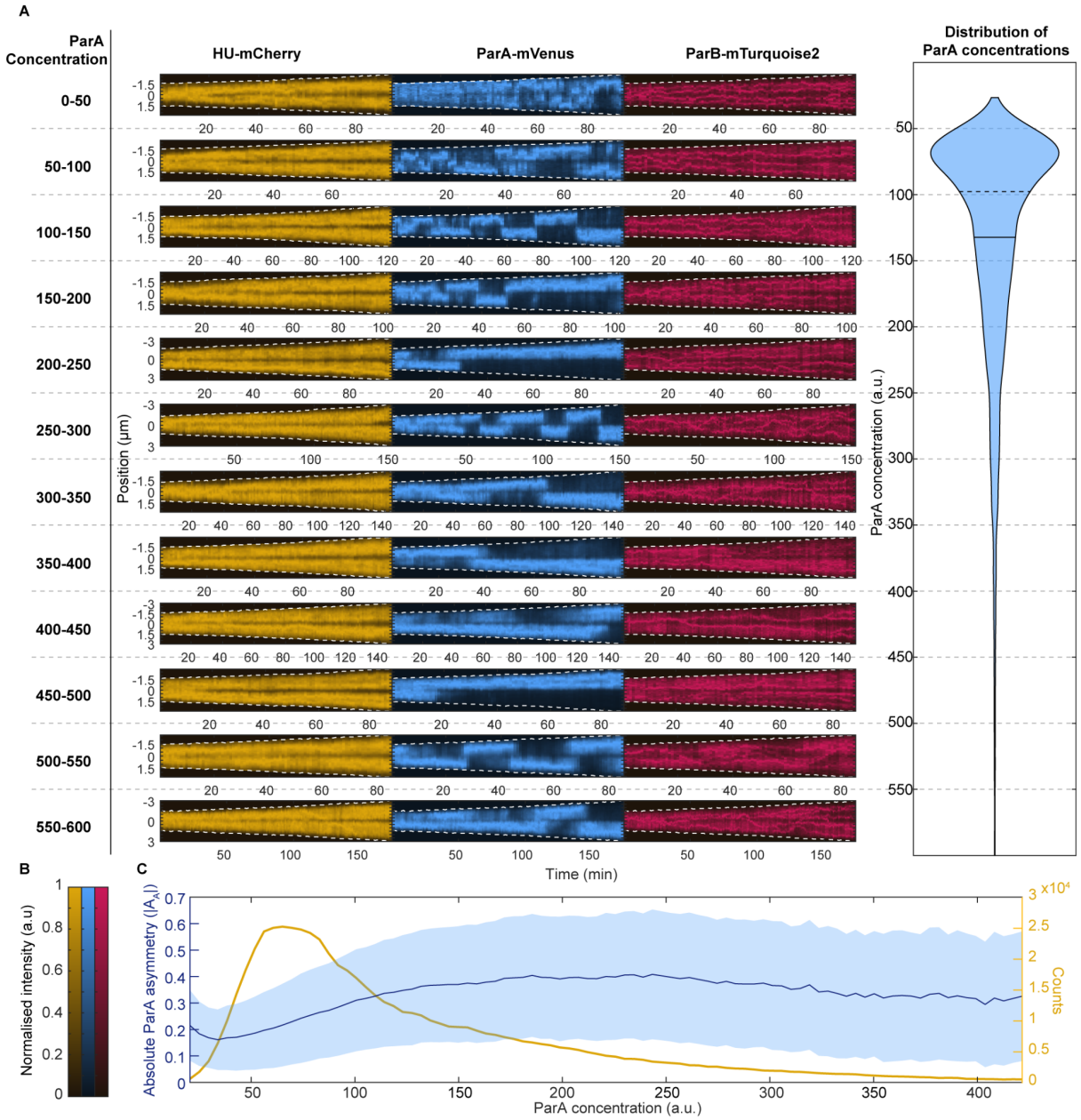

Figure S3. **(A)** Cell cycles showcasing diverse ParA concentrations. Presented here are 12 cell cycles, each representing an interval of ParA concentrations from low to high. Each example features a kymograph depicting nucleoid (HU-mCherry), ParA, and ParB signal. Adjacent to this, a violin plot provides an overview of the overall ParA concentration distribution. The displayed distribution represents the average ParA concentration from birth to division of each cell cycle, calculated by integrating the ParA signal and then dividing by the area of the cell. The horizontal dashed line represents the median, while the continuous line signifies the mean. **(B)** Colour scales for **(A)**. **(C)** In blue: Average absolute ParA asymmetry (continuous line) ± standard deviation (shaded area) plotted against ParA concentration. In orange: Number of data points. The violin plot in **(A)** and panel **(C)** were generated from 5219 cell cycles.

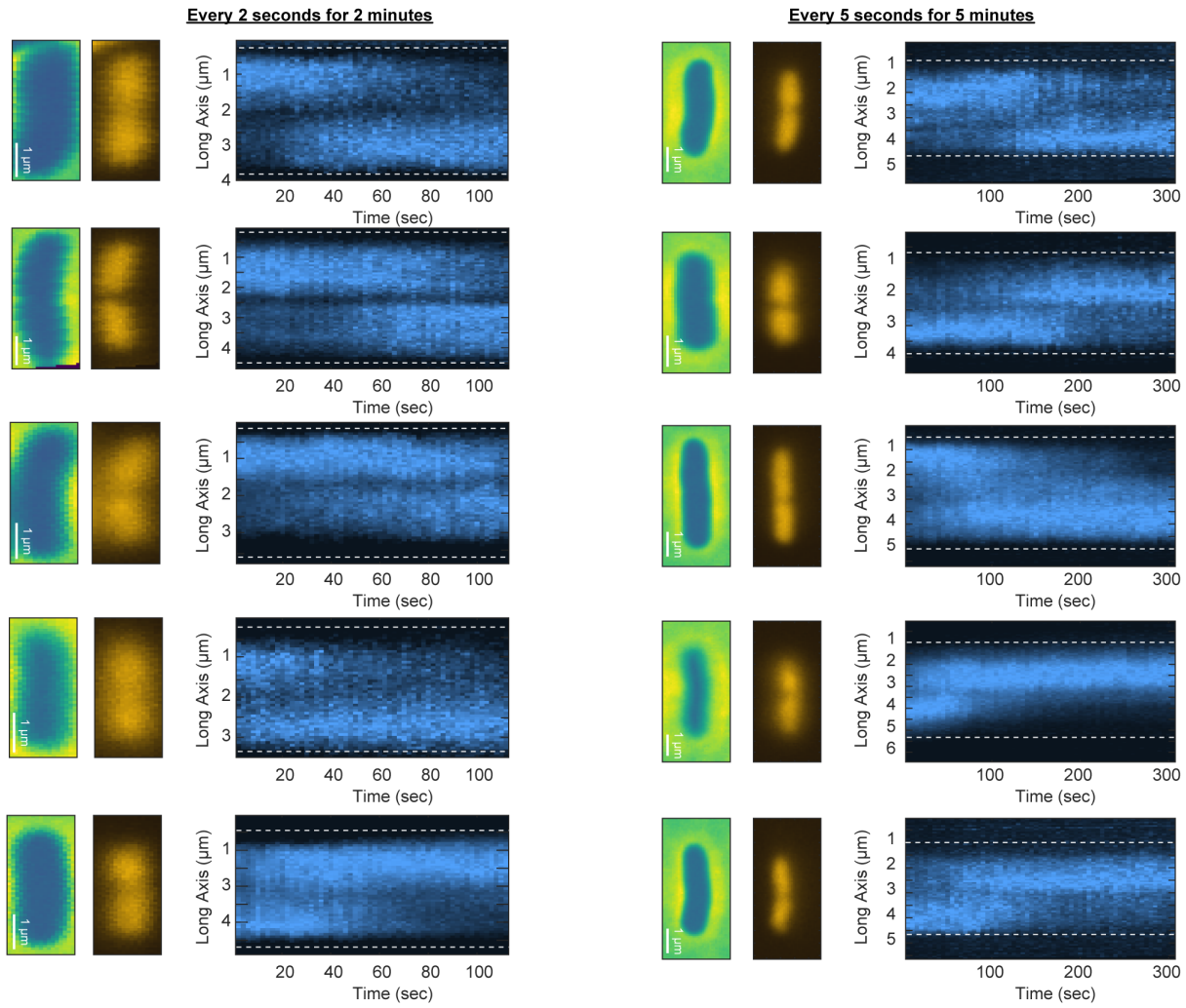

Figure S4. ParA kymographs with high temporal resolution: Left: ParA signal was captured every 2 seconds over 2 minutes. Right: ParA signal was captured every 5 seconds over 5 minutes. Shown are, in order, phase contrast, nucleoid, and ParA profile along the long axis of the cell.

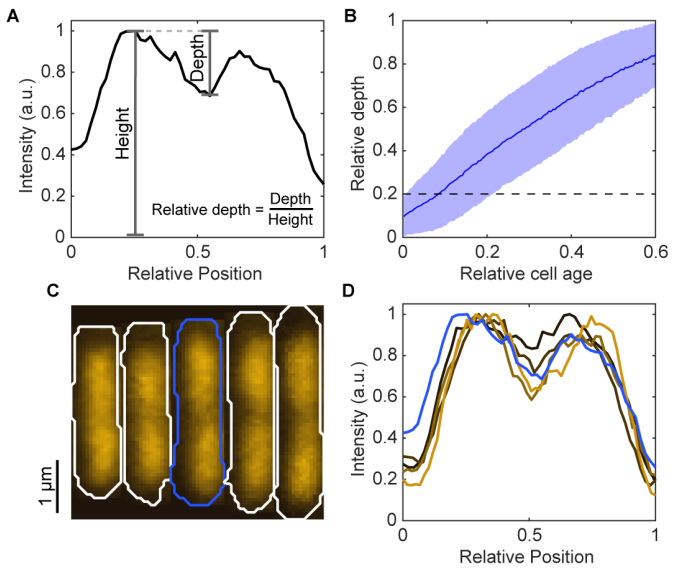

Figure S5. Nucleoid constriction detection. **(A)** Example of an intensity profile of HU-mCherry. Highlighted are the height (max intensity) and the depth (distance between height and valley) and how to calculate the relative depth. **(B)** Average relative depth plotted against relative cell age; shade region is the standard deviation. The dashed line indicates the threshold depth for nucleoid constriction detection, defined as the 95% percentile of all relative depths on the first frame of each cell cycle (n=5219). This definition attempts to exclude random dips in the nucleoid and is based on the assumption that almost no cells have a genuine constriction at birth under slow growth conditions. **(C)** Example of nucleoid constriction formation. The cell outlined in blue indicates the initial instance where a nucleoid constriction was detected, and this feature persists in all subsequent cells. **(D)** Line profiles of the 5 cells shown **(C)**. The blue line corresponds to the cell with the blue outline.

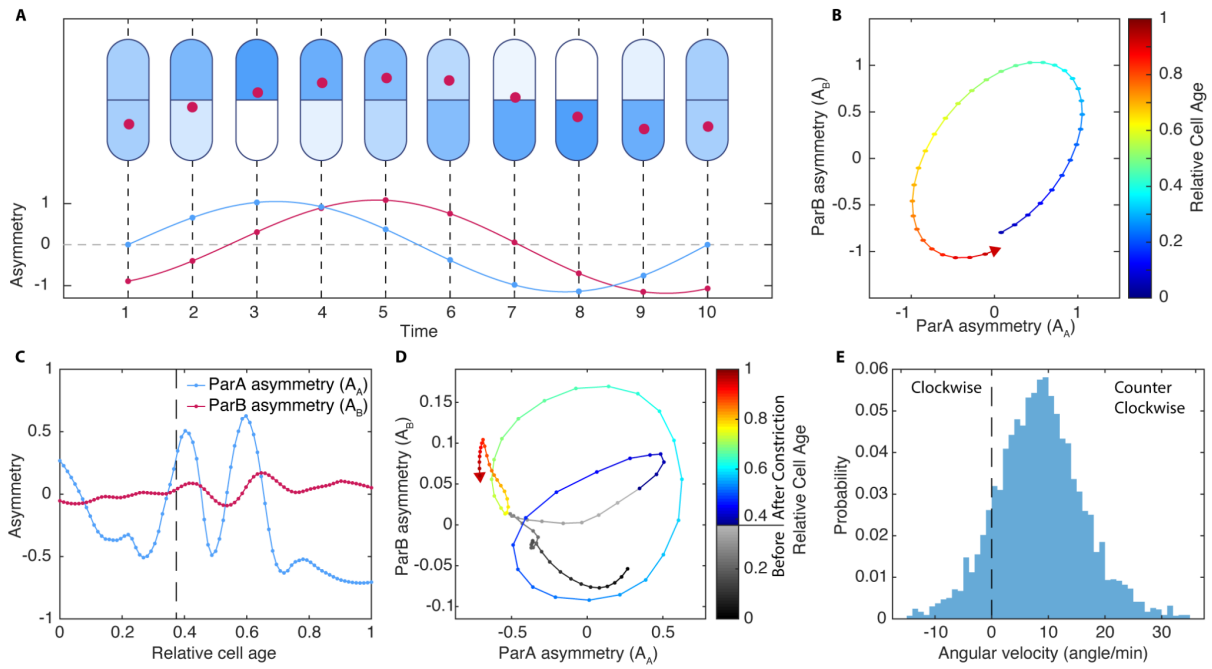

Figure S6. The dance of ParA and ParB. **(A)** Cartoon representation of the asymmetry between ParA (blue) and ParB (red) in a bacterial cell. Top: A cell with one ParB-coated plasmid actively chasing ParA. Bottom: the time series of the asymmetry of both ParA (A_A) and ParB (A_B). **(B)** Asymmetry plot: Trajectory of the interplay between ParA and ParB asymmetry. The colour shows relative cell age ranging from 0 (birth/blue) to 1 (division/red). **(C)** Asymmetry of ParA and ParB of a real cell cycle. The dashed line indicates the time point when a nucleoid constriction was first detected. Both curves were smoothed using a robust locally weighted scatterplot smoothing algorithm with a smoothing parameter of 0.2 to transform the curves into more wave-like forms. **(D)** The asymmetry plot of the same cell cycle as in **(C)**. The colour shows relative cell age, with grey indicating data points prior to nucleoid constriction. **(E)** A histogram of the angular velocity after the nucleoid constriction was detected. Angular velocities were calculated from trajectories of ParA and ParB asymmetry, similar to the trajectory shown in **(D),** of 5219 cell cycles.

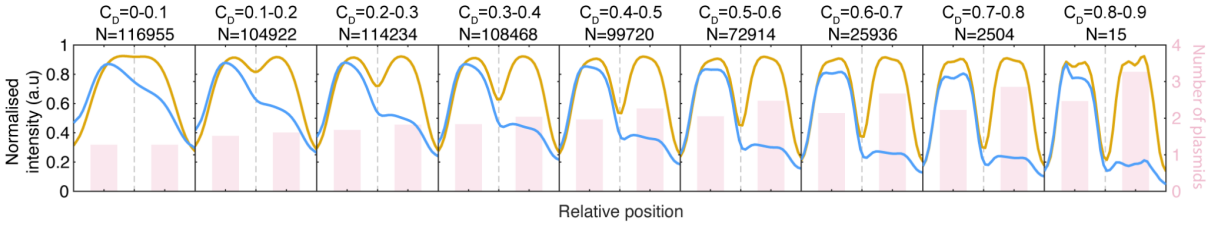

Figure S7. ParA flips create a sharp gradient of ParA across the nucleoid constriction. Normalised profiles of nucleoid and ParA (with max values set to 1 before averaging) for different constriction depths C_D (0 indicates no constriction, 1 indicates complete separation/ no HU-mCherry signal between the lobes of the nucleoid). Cells were oriented such that the majority of ParA is in the same cell half. Light red bars in the background depict the average plasmid count in each cell half.

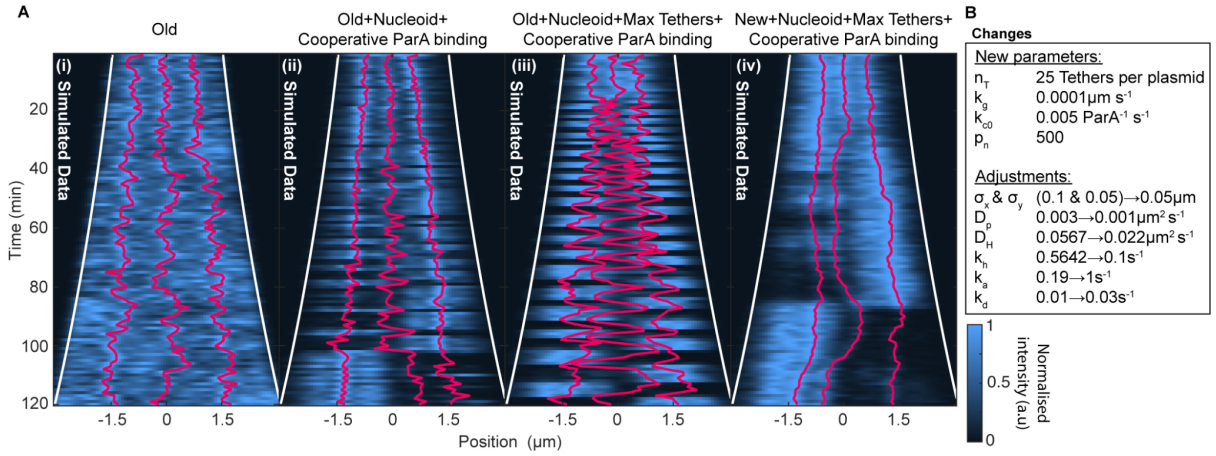

Figure S8. New and adjusted parameters. **(A)** Kymographs of simulations with different parameters. (i): Parameters from Köhler et al., (ii): Parameters from Köhler et al. with the inclusion of a nucleoid and cooperative ParA binding, (iii): As in (ii) but with a limit on the number of ParA-ParB tethers, (iv) As in (iii) but with newly adjusted parameters. **(B)** New parameters that were introduced to the model: (n_T) Upper limit of ParA-ParB tethers per plasmid was set based on *in vivo* observations indicating no ParA foci at the plasmid's position. This also enhances plasmid mobility. (k_g) Growth rate of the cell. (k_c) Rate of cooperative ParA binding, (p_n) Attraction of ParA to the nucleoid was determined by matching the distribution of ParA within real and simulated cells. Adjusted parameters that were changed to mimic *in vivo* observations by reducing the mobility of the plasmid (k_h, D_P & $\sigma_{x,y}$) and by reducing the frequency of ParA flips (D_H & k_d) and by adjusting background levels of ParA (k_a).

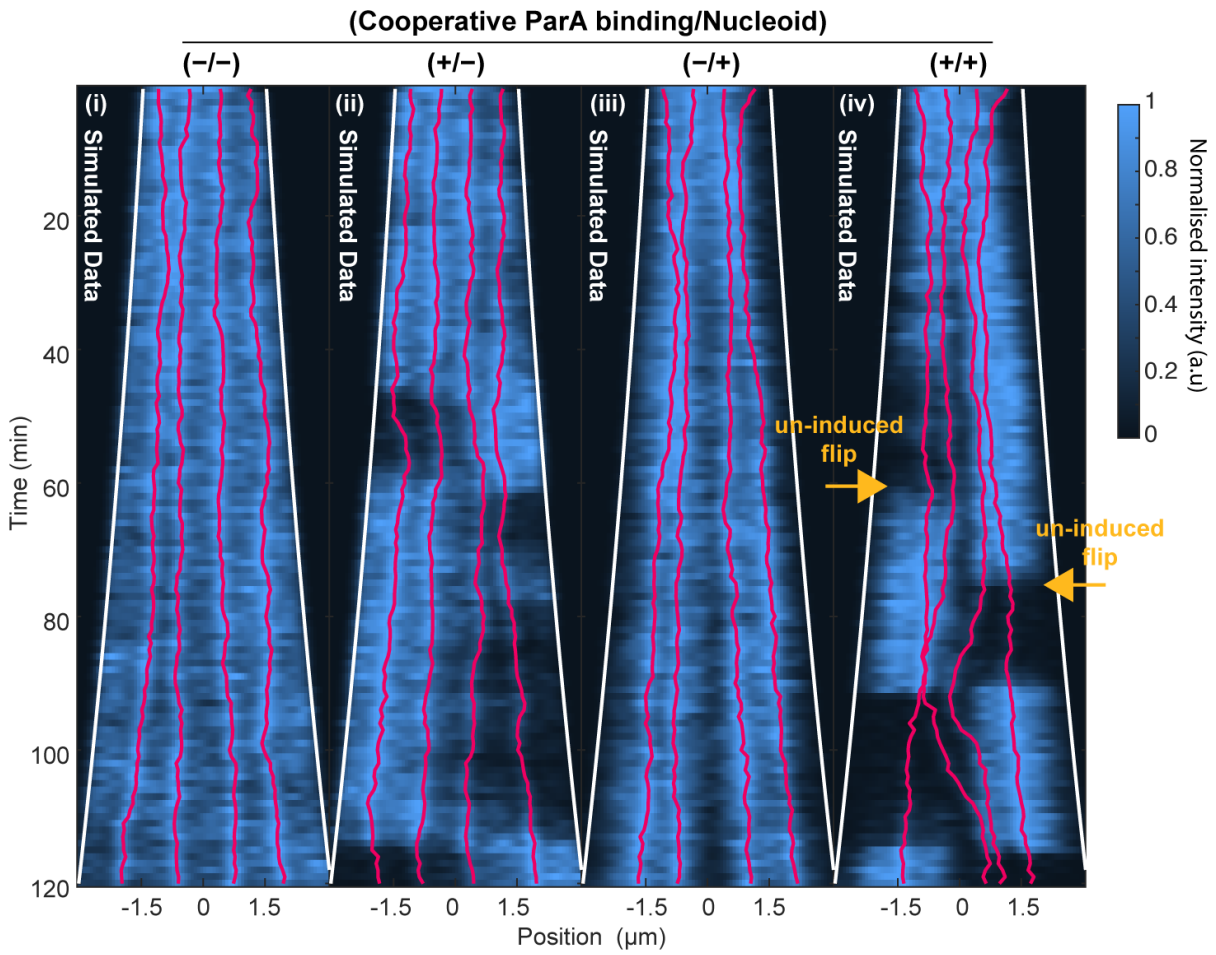

Figure S9. Cooperative ParA binding causes instability of ParA at even plasmid numbers. Simulations with four conditions similar to Figure 4C but with four plasmids instead of 3. In (iv) the orange arrows indicate where the ParA does an un-induced flip (no plasmid crossing mid-cell preceding the flip).